

**Reviewer comment:**

*The methodical part of the back trajectory analysis in section 3 is still insufficient. There is very little or almost no information given how exactly the back trajectories are used for calculation of the immission maps. It seems that the emissions were summed up all along the trajectory without taking the height of the trajectory into account or whether the air parcel had contact with the PBL and a chance to pick up emissions or not. Although I am not an expert on back trajectory analysis, I would consider this issue very essential for the paper. For linking emissions with concentration maps (immission maps) only emissions from grid cells where the back trajectory was close to the ground should be considered. If this is not the case here, I would have doubts regarding the validity and the usefulness of the calculated immission maps and consequently of the key messages of this paper. So it is in my view crucial that the applied back trajectory analysis has been done correctly. This must be demonstrated by a more detailed and convincing description of the applied method.*

**Response:**

We fully agree with the reviewer as to the missing crucial information about our use of the trajectories. We are very sorry that this information somehow got lost in the course of our revisions. It was maintained though in the caption to the maps.

We now complemented section 3 with the crucial sentence:

“In the immission maps constructed with extrapolated measurements at the stations and in any comparisons with emissions along the back trajectories only trajectory points under 1000 m altitude above ground were utilized. “

# **Aerosol immission maps and trends over Germany with hourly data at four rural background stations from 2009 to 2018**

Jost Heintzenberg<sup>1</sup>, Wolfram Birmili<sup>2</sup>, Bryan Hellack<sup>2</sup>, Gerald Spindler<sup>1</sup>, Thomas Tuch<sup>1</sup>, and Alfred Wiedensohler<sup>1</sup>

1: Leibniz Institute for Tropospheric Research (TROPOS), Permoserstr. 15, 04318 Leipzig, Germany

2: German Environment Agency, Wörlitzer Platz 1, 06844 Dessau-Roßlau, Germany

## **Abstract**

Ten years of hourly aerosol and gas data at four rural German stations have been combined with hourly back trajectories to the stations and inventories of the European EDGAR emission database yielding immission maps over Germany of PM<sub>10</sub>, particle number concentrations, and equivalent black carbon (eBC). The maps reflect aerosol emissions modified with atmospheric processes during transport between sources and receptor sites. Compared to emission maps strong Western European emission centers do not dominate the downwind concentrations because their emissions are reduced by atmospheric processes on the way to the receptor area. PM<sub>10</sub>, eBC, and to some extent also particle number concentrations are rather controlled by emissions from Southeastern Europe from which pollution transport often occurs under dryer conditions. Newly formed particles are found in air masses from a broad sector reaching from Southern Germany to Western Europe which we explain with gaseous particle precursors coming with little wet scavenging from this region.

Annual emissions for 2009 of PM<sub>10</sub>, BC, SO<sub>2</sub>, and NO<sub>x</sub> were accumulated along each trajectory and compared with the corresponding measured time series. The agreement of each pair of time series was optimized by varying monthly factors and annual factors on the 2009

Gelöscht:

Gelöscht: necessarily

29 emissions. This approach yielded broader summer emission minima than published values that  
30 were partly displaced from the midsummer positions. The validity of connecting immission  
31 and emission of particulate pollution was tested by calculating temporal changes of eBC for  
32 subsets of back trajectories passing over two separate prominent emission regions, region A to  
33 the Northwest and B to the Southeast of the measuring stations. Consistent with reported  
34 emission data the calculated immission decreases over region A are significantly stronger than  
35 over region B.

**Gelöscht:** For BC, SO<sub>2</sub>, and NO<sub>x</sub> stronger emission-reductions were determined than what German and European environmental agencies reported. These findings are emphasized with 2017 as endpoint of the trend from which on our study shows emission increases. Comparing calculated trends with emission trends in neighboring countries as published by EEA supports the explanation that the observed trends are to some extent due to changes in imported air masses. Most strongly this holds for SO<sub>2</sub>, the trend of which follows that of Romanian emissions rather well.

## 1 Introduction

The atmospheric aerosol is known to influence the Earth's radiation budget because it directly scatters and absorbs solar radiation (Schwartz, 1996; Bond et al., 2013), and acts as cloud condensation nuclei, thus modulating the optical properties and lifetimes of clouds (Twomey, 1974; Penner et al., 2004). In many regions of the globe that had undergone industrialization early on, anthropogenic aerosol concentrations are currently in decline (Leibensperger et al., 2012; Zanatta et al., 2016). With respect to declining concentrations and emissions, Samset al. (2018) suggest that removing present-day anthropogenic aerosol emissions – assuming constant greenhouse gas emissions, could lead to a global mean surface heating as high as 0.5–1.1°C.

Besides climate, the atmospheric aerosol has been acknowledged to influence human health through respiratory and cardiovascular health endpoints (Anderson et al., 2012). Lelieveld et al. (2015) quantified the world-wide burden of disease (premature mortality) due to outdoor pollution, large part of which was attributed to airborne particulate matter. It is apparent that the distribution of adverse health effects is very uneven among the world-wide population, depending on the local level of outdoor pollution.

In view of the described man-driven effects it seems imperative to develop instruments to reliably monitor changes in anthropogenic aerosol concentrations as well as an understanding of the balance between aerosol sources and measured concentrations. Researchers have strived to obtain a spatial picture of the distribution of pollutants, and to achieve a connection between the sources of pollution and concentrations downwind. A widely used method has been the extrapolation of concentrations measured in one or several locations into two-dimensional space through the use of meteorological dispersion approaches: The first maps of particulate

Formatiert: Rechtschreibung und Grammatik prüfen

Formatiert: Rechtschreibung und Grammatik prüfen

Formatiert: Rechtschreibung und Grammatik prüfen

Formatiert: Rechtschreibung und Grammatik prüfen

73 air pollutants over Europe were constructed in the 1970s with the help of coarse emission data  
74 and simple trajectory models (Eliassen, 1978). Statistical methods were developed to connect  
75 pollution sources and ensuing aerosol concentrations at receptor sites (Miller et al., 1972;  
76 Friedlander, 1973; Cass and McRae, 1983). By combining statistics with back trajectory data  
77 sectorial information about sources controlling the composition of the aerosol over Southern  
78 Sweden was derived by Swietlicki et al., (1988). Later the approach of using back trajectories  
79 to map aerosol sources was refined by Stohl (1996) and tested with one-year sulfate data from  
80 the co-operative program for monitoring and evaluation of the long-range transmission of air  
81 pollutants in Europe (EMEP, [www.emep.int](http://www.emep.int)). In a similar approach with five years of aerosol  
82 data from a single Siberian receptor site Heintzenberg et al. (2013) identified potential source  
83 regions over Eurasia and with aerosol data from four Swedish icebreaker expeditions over the  
84 Central Arctic (Heintzenberg et al., 2015). Charron et al. (2008) constructed concentration field  
85 maps to identify the source regions of specific types of aerosol particle size distributions  
86 arriving in England. All these works share the approach that time-dependent information on  
87 concentrations measured at receptor site(s) are transformed into space, thus allowing  
88 conclusions on the potential source regions of gaseous and/or particulate emissions.

89

90 With more comprehensive air quality models concentrations of specific aerosol were  
91 mapped over Europe together with short temporal developments (e.g., Schell et al., 2001). For  
92 specific episodes high spatial resolution aerosol concentration maps in urban and non-urban  
93 European areas have been generated with sophisticated chemistry transport models (e.g.,  
94 Beekmann et al., 2015; Riemer et al., 2004; Wolke et al., 2004). For the years 2002 and 2003  
95 Marmer and Langman (2007) analyzed the spatial and temporal variability of the aerosol  
96 distribution over Europe with a regional atmosphere-chemistry model. They found that  
97 meteorological conditions play a major role in spatial and temporal variability in the European  
98 aerosol burden distribution. Regionally, year to year variability of modeled monthly mean

Formatiert: Rechtschreibung und Grammatik prüfen

aerosol burden reached up to 100% because of different weather conditions.

In the present study ten years of hourly aerosol data at four German stations were available for the identification of potential source regions. As it appears unrealistic to analyze such a large database with advanced chemical transport models we resorted to the well proven approach of utilizing back trajectories cited above and connected the results to emission fields. We define the resulting concentration maps of particulate and gas parameters as immission maps because they represent long-term average emissions of air pollutants modified by the controlling atmospheric processes along the pathways to the receptor sites. In Charron et al. (2008) this approach is termed “concentration field map method”. With a much larger data set spanning a much tighter network of 1500 stations Rohde and Muller (2015) used the Kriging interpolation approach (Krige, 1951) to construct air pollution maps over China. Another approach to construct pollution maps over the province Henan, China was used by Liu et al., (2018). They combined an emission inventory with chemical modeling and back trajectories to derive high resolution maps of particulate and gaseous pollution components and find that emissions from neighboring provinces are important contributors to local air pollution levels.

Recent political, economic and technological developments in Europe have caused substantial changes in the emission of air pollutants. Lavanchy et al. (1999) deduced a trend in atmospheric black carbon from preindustrial times to 1975. Strong downward trends in major aerosol components before and after the German reunification (1983-1998) over rural East Germany were reported by Spindler et al., (1999). For the years 2003 – 2009 Kuenen et al., (2014) published trends in the development of aerosol emissions as elaborated from reported emissions. The German Environmental Agency (GEA) publishes trends in air pollution as measured at a number of ca. 380 federal and state air quality stations (Minkos, 2019).

Gelöscht:

Formatiert: Rechtschreibung und Grammatik prüfen

125 According to these records, PM<sub>10</sub> mass concentrations declined by approximately 25 % over  
126 the period 2000-2019

127

128 Combining long-term aerosol and gas data at the four stations of the present study provide  
129 an excellent data base for identifying both the most important source regions and possible  
130 temporal changes. During the ten recent years covered by our data we expected noticeable  
131 systematic changes in our time series that can be interpreted in terms of emissions. As a side  
132 result in the process of deriving long-term emission trends of major air pollutants over Germany  
133 information of the monthly disaggregation of annual aerosol emissions can be derived.

134

135

## 136 2 Aerosol and trace gas data

137

138 The core data of the present study have been measured at the stations Melpitz (ME),  
139 Neuglobsow (NG), and Waldhof (WA) of the German Ultrafine Aerosol Network GUAN  
140 network (Birmili et al., 2016) and at station Collmberg (CO) operated by the Saxonian  
141 Environment Agency. These four rural background stations lie in the northeastern lowlands of  
142 Germany at distances between 30 and 205 km from each other. Ten-year-average particle mass  
143 concentrations under 10 µm particle diameter (PM<sub>10</sub>) and their standard deviations at the four  
144 stations are rather similar: 15±13, 22±12, 14±10, and 15±11 µgm<sup>-3</sup> at CO, ME, NG, and WA,  
145 respectively. The corresponding long-term average particle number concentrations between 10  
146 and 800 nm particle diameter (N<sub>10-800</sub>) and their standard deviations at the three GUAN-stations  
147 are 5400±4100, 3600±2300, and 4300±2800 cm<sup>-3</sup>, respectively. Basic statistics on particle  
148 number and eBC mass concentrations of the three GUAN-stations were presented in Sun et al.  
149 (2019) whereas details about instrumentation and their maintenance can be found in Birmili et

**Gelöscht:** Table 1 gives an overview over their characteristics.

al., (2016). The ensemble of hourly data at the four stations is the base of the pollution maps derived in this work.

TROPOS-type mobility particle size spectrometers (MPSS, Wiedensohler et al., 2012) were used to record particle number size distributions across the particle size range 10-800 nm. Quality assurance of the long-term measurements followed the recommendations of Wiedensohler et al. (2018) including weekly inspections as well as monthly and annual maintenance intervals. Once a year the MPSS were intercompared against a reference MPSS of the WCCAP (World Calibration Center for Aerosol Physics) either on-site and/or at the calibration facility. The lower detection limit of the MPSS is around 30 cm<sup>-3</sup> for a time resolution of 30 minutes. Equivalent Black Carbon (eBC) was determined by multi-angle absorption photometers (MAAP) using a mass absorption cross section of 6.6 m<sup>2</sup> g<sup>-1</sup> (Petzold et al., 2013; Nordmann et al., 2013; Birmili et al., 2016). An intercomparison of multiple MAAP instruments resulted in an inter-device variability of less than 5% (Müller et al., 2011). While the MAAP deployed at the TROPOS station Melpitz was biannually compared to the reference absorption photometer at the WCCAP in Leipzig, the instruments at the UBA stations Waldhof and Neuglobsow were serviced by the manufacturer. For hourly measurements of PM<sub>10</sub> continuous oscillating microbalances (Thermo Scientific TEOM 1400) were utilized at stations CO, NG, and WA. At station ME PM<sub>10</sub> was determined in daily filter samples (0:00 to 24:00 CET), Spindler et al. (2013). The TEOM1400-instrument and gravimetric filter sampling are different methods for particle mass concentrations. The TEOM collects particulate mass on a vibrating substrate (tapered element) and registers the change of the oscillation frequency that is decreasing with mass loading (Patashnick and Rupprecht, 1991). The TEOM operates at a constant temperature setting above ambient (typically 30– 50°C) to prevent contraction and expansion of the tapered element and reduce interferences from water vapor condensation. However, heating the ambient air enhances volatilization of particle-

Formatiert: Hochgestellt

Gelöscht: data were



bound semivolatile compounds (e.g., ammonium nitrate and some organic species) resulting in an underestimation of PM when semivolatile material dominates the particulate phase during cold seasons. The condensation and evaporation of ammonium nitrate and organic species can also influence the filter sampling under ambient conditions. Here the effect can be balanced partly by the temperature variation during the daily filter sampling. However, the results of both methods mostly are in good agreement (e.g., Zhu et al., 2007).

Hourly aerosol data from the three GUAN-stations during 2009 – 2015 ( $NG \geq 2011$ ) have been utilized in a previous study (Heintzenberg et al., 2018) to understand aerosol processes during air mass transport between the stations. In the present study the data set was enlarged to include the additional station Collmberg and data at all stations from the year 2016 through 2018. The integral aerosol parameters particle number concentration ( $N_{10-800}$ ,  $\text{cm}^{-3}$ ), light absorption-equivalent mass concentration of Black Carbon (eBC,  $\mu\text{g m}^{-3}$ ), and particle mass concentrations under  $10 \mu\text{m}$  particle diameter ( $\text{PM}_{10}$ ,  $\mu\text{g m}^{-3}$ ) were utilized.  $N_{10-800}$  is based on the integral over measured particle size distributions from 10 to 800 nm.

$\text{NO}_x$  and  $\text{SO}_2$  emitted by anthropogenic combustion processes are transformed in the atmosphere and add to the anthropogenic aerosol. At the three GUAN stations both are measured with the same temporal resolutions as the aerosol data. Additionally, at Collmberg  $\text{NO}_x$ -data could be utilized in the interpretation of the aerosol data. The trace gas analyzers for  $\text{NO}_x$  and  $\text{SO}_2$  were calibrated with test gases for NO (NO in  $\text{N}_2$ ) and  $\text{SO}_2$  ( $\text{SO}_2$  in  $\text{N}_2$ , both Air Liquide, Germany).  $\text{NO}_2$  was produced in a gas phase titration device (GPT APMC370, Horiba, Germany) by quantitative oxidation of NO test gas (Rehme, 1976). The trace gas analyzers were used in an optimal range and all registered values (also below the detection limit) were used for this long-term study. As most particle numbers in polluted continental environments tropospheric ozone is a secondary atmospheric pollutant. We utilized hourly

**Gelöscht:** s

**Gelöscht:** Of the total number of 87648 hours during the ten-year period 77516 hours with at least concurrent  $\text{PM}_{10}$ -data at all four stations could be utilized.

**Gelöscht:** number concentrations below 10 - 26 nm ( $N_{10-26}$ ,  $\text{cm}^{-3}$ ), and

**Gelöscht:** Both,

**Gelöscht:** and  $N_{10-26}$  are

**Gelöscht:** s

**Formatiert:** Schriftart: Nicht Kursiv, Englisch (USA)

**Formatiert:** Schriftart: Nicht Kursiv, Englisch (USA), Tiefgestellt

**Formatiert:** Schriftart: Nicht Kursiv, Englisch (USA)

**Formatiert:** Schriftart: Nicht Kursiv, Englisch (USA), Tiefgestellt

**Formatiert:** Schriftart: Nicht Kursiv, Englisch (USA)

**Gelöscht:** Through combustion processes the trace gases  $\text{NO}_x$  and  $\text{SO}_2$  are related to anthropogenic aerosol formation

**Gelöscht:** ,

**Gelöscht:** (cf. Table 1 for instrumental details).

**Formatiert:** Tiefgestellt

**Formatiert:** Tiefgestellt

**Formatiert:** Tiefgestellt

**Formatiert:** Tiefgestellt

**Formatiert:** Tiefgestellt

**Formatiert:** Tiefgestellt

**Formatiert:** Tiefgestellt

ozone data taken at all four stations throughout the studied time period as ancillary information in the discussion of particle-number related results. For the ozone measurements a common trace gas ozone monitor was used (Horiba APOA-350). This device quantifies tropospheric ozone by UV Absorption and use the cross-flow modulation principle. Ambient air with and without ozone (elimination by a selective scrubber) was used alternatively in the measuring cuvette yielding a very stable ozone signal. The devices were calibrated using an ozone-standard (Ozon-Calibrator, Thermo Environmental Instruments 49PS).

Table 1 gives an overview over the instrumental characteristics of all stations and the total number of validated data hours for each utilized component. The minimum is 57962 hours for validated MPSS-data at the three GUAN-stations and the maximum with 88838 validated data hours for  $\text{NO}_x$  at all four stations. Strictly concurrent (by the hour) are less validated data hours. For MPSS, eBC, and  $\text{SO}_2$ -data at the GUAN-stations this numbers is 48533 hours, and 48114 and 47729 hours for  $\text{PM}_{10}$  and  $\text{NO}_x$ -data, respectively, at all four stations. However, these reduced strictly concurrent numbers do not substantially affect the 10-year-average maps discussed below.

Formatiert: Tiefgestellt

Formatiert: Tiefgestellt

Formatiert: Tiefgestellt

Formatiert: Tiefgestellt

Gelöscht:

### 3 Back trajectories

With the HYSPLIT4 model (Stein et al., 2015) and based on the meteorological fields from the Global Data Assimilation System with one-degree resolution (GDAS1, <https://www.emc.ncep.noaa.gov/gmb/gdas/>) three-dimensional trajectories were calculated arriving every hour at a height of 500m above ground level at the four stations. The trajectories were calculated backward for up to five days using the meteorological fields from the server at

244 Air Resources Laboratory (ARL), NOAA (<http://ready.arl.noaa.gov>), where more information  
 245 about the GDAS dataset can be found. In the immission maps constructed with extrapolated  
 246 measurements at the stations and in any comparisons with emissions along the back trajectories  
 247 only trajectory points under 1000 m altitude above ground were utilized. Turbulent  
 248 atmospheric mixing is included in parameterized form in HYSPLIT4. The present study  
 249 utilizes the default version of this parameterization according to Draxler and Hess (1998). The  
 250 back trajectories are calculated with the base version of HYSPLIT4 that does not include any  
 251 specific dispersion and scavenging of atmospheric trace substances. Precipitation along the  
 252 trajectories was used in the interpretation of the immission maps. The precipitation values  
 253 mapped in the present study and the temperature values used in the trend discussion of  $N_{10-800}$   
 254 are those listed by HYSPLIT4 at each point of a trajectory. They are meteorological parameters  
 255 at the nearest grid cell of the assimilated global meteorological fields provided by the U.S.  
 256 National Weather Service's National Centers for Environmental Prediction (NCEP)  
 257 (Kanamitsu, 1989). Average horizontal wind speeds in between two one-hour trajectory steps  
 258 were calculated from the distance covered by a trajectory between two successive steps. With  
 259 the 350593 hourly back trajectories from the four stations the time series of  $N_{10-800}$ ,  $PM_{10}$ , and  
 260 eBC were extrapolated over Germany and part of the neighbor countries. At Melpitz  $PM_{10}$ -  
 261 data were only available as daily averages. Thus, the daily average concentrations were  
 262 extrapolated along each hourly trajectory of the respective day.

263

264

#### 265 4 Emission data

266

267 For the interpretation of the immission maps we used the emission data set version 4.3.2 for  
 268 2009 of the components particle mass concentrations below  $10\ \mu m$  ( $PM_{10}$ ), BC,  $NO_x$  and  $SO_2$

Formatiert: Englisch (USA)

Formatiert: Englisch (USA)

Formatiert: Englisch (USA)

Formatiert: Tiefgestellt

Gelöscht: given

Gelöscht: is just the

Gelöscht: precipitation rate

Gelöscht: taken from the GDAS1-fields

Formatiert: Englisch (USA)

Formatiert: Rechtschreibung und Grammatik prüfen

Gelöscht: used by HYSPLIT where the trajectory is located and does not depend on the cloud value at the height of the trajectory

Gelöscht: derived

Gelöscht: the

Gelöscht:  $N_{10-26}$

279 as compiled in the Emissions Data Base for Global Atmospheric Research (EDGAR,  
280 [https://edgar.jrc.ec.europa.eu/overview.php?v=432\\_AP](https://edgar.jrc.ec.europa.eu/overview.php?v=432_AP), DOI ([https://data.europa.eu/doi/10.2904/JRC\\_DATASET\\_EDGAR](https://data.europa.eu/doi/10.2904/JRC_DATASET_EDGAR)). This data set concerns primary emissions only and has been  
281 introduced by Crippa et al., (2018). All human activities, except large scale biomass burning  
282 and land use, land-use change, and forestry are included in the data base. Emissions of coarse  
283 particles from agricultural surfaces are not included. They are, in fact, very sensitive to soil  
284 and weather conditions, and thus not trivial to quantify. Primary aerosol emission data are  
285 generally characterized by rather high uncertainties. For the EDGAR data base Crippa et al.  
286 (2018) report a range of variation in 2012 between 57.4% and 109.1% for PM<sub>10</sub>, and between  
287 46.8% and 92% for BC. Even higher uncertainties in PM emissions might come from super-  
288 emitting vehicles that are not considered in this data base (Klimont et al., 2017). In our maps  
289 and trend calculations we applied the grid values of emission data that were listed in the  
290 EDGAR inventories no more than 30 km away from any trajectory time step.

Formatiert: Tiefgestellt

Gelöscht: This emission data set has been introduced by Crippa et al., (2018).

Formatiert: Rechtschreibung und Grammatik prüfen

## 294 5 Results and discussion

### 295 5.1 Aerosol concentration maps (immission maps)

296 The trajectory-extrapolated N<sub>10-800</sub>, PM<sub>10</sub>, and eBC from the four stations yielded immission  
297 maps averaged over the period 2009 – 2018, that are collected in Figs. 1-2. Both, the particle-  
298 number related N<sub>10-800</sub> and the particle-mass related PM<sub>10</sub>, and eBC exhibit systematic seasonal  
299 variations. Most events of new particle formation (NPF) over the continents occur during the  
300 photochemically active summer months (Kulmala et al., 2004) whereas the particle-mass  
301 related aerosol parameters due to combustion processes exhibit highest concentrations during  
302 the winter months (Matthias et al., 2018). Consequently, we constructed two maps for each  
303 discussed component: One of averages over the months April through October and one of

Gelöscht: N<sub>10-26</sub>,

averages over the months November through March. Only map cells with at least 300 trajectory hits are discussed. Interpreting these hits in terms of Poisson-statistics would then yield a maximum uncertainty of 5.8% per cell. In terms of a Gaussian statistic the arithmetic cell-averages displayed in the maps exhibit standard deviations of cell averages that are less than six percent.

The maps of  $N_{10-800}$  in Fig. 1 show distributions of air masses over Germany and adjacent countries related to particle numbers instead of particulate mass. There are two arguments for showing maps of number related results. First, particle number concentrations are connected with cloud processes, their formation (Pruppacher and Klett, 1978), radiative effects, e.g., albedo (Twomey, 1974), and precipitation (Li et al., 2011). Second, in the area of aerosol-health issues ultrafine particles ( $< 100$  nm diameter) have been gaining attention in recent years (Wichmann and Peters, 2000), i.e. an increasing number of health effects is attributed rather to particle number than to particle mass. The fact that NPF-events occur concurrently in or near the top of the continental planetary boundary layer over wide geographical regions (e.g., Wehner et al., 2007) is partly due to concurrent advantageous photochemical conditions allowing for the formation of condensable vapors, in particular global radiation (Birmili et al., 2001). Two other factors constraining NPF are the availability of gaseous particle-precursors and the concurrent pre-existing aerosol.

The summer map (4-10) of  $N_{10-800}$  exhibits the high values in the Southwest-to-Northeast-sector of the map. Highest values are concentrated in a belt reaching from Burgundy through Switzerland, Southern Germany, Czech Republic to Southwestern Poland. Interestingly, this belt of high  $N_{10-800}$  is collocated to large extent with a belt of high summer ozone concentrations (cf. Fig. S1). This photochemically controlled pollutant (Monks et al., 2015) exhibits highest summer concentrations in air masses from Southwestern Poland and Northern Czech Republic.

**Gelöscht:** (Kulmala et al., 2004)(Matthias et al., 2018)

**Gelöscht:** The highest map-coverage was reached with  $PM_{10}$  with at least 3951 data points in each geocell. As eBC and size distribution data were only available at the three GUAN-stations the derived maps contained a minimum of 751 data points per geocell.

**Gelöscht:** s

**Gelöscht:** ,

a region from which high ozone values are reported (Struzewska and Jefimow, 2013; Hůnová, 2003; Hůnová and Bäumelt, 2018). However, the summer map of  $N_{10-800}$  does not show the highest values in air masses from the region with highest ozone pollution. High particle numbers in air masses coming over the Alps from Northern Italy may be related to the high emissions of air pollutants in the Po Valley that are known to reach frequently through so called alpine pumping (Winkler et al., 2006; Lugauer and Winkler, 2005; Reitebuch et al., 2003) over the mountains. The high  $NO_x$ -concentrations in air masses from Northern Italy in both summer and winter maps (see Fig. S2) indicate that pollution from south of the Alps can even reach Northeastern Germany. In the winter map of  $N_{10-800}$  (11-3 in Fig. 1) the belt of highest summer values is apparently complemented by more transalpine pollution transport and by transport from the Southeast. The lower photochemical activity in winter is reflected in the lower winter ozone concentrations in Fig. S1, albeit transalpine pollution transport is still visible in the winter map of  $NO_x$  in Fig. S2. Northwestern Italy also shows up as an emission hot spot in the maps of trajectory-summed emissions in Fig. S4.

Formatiert: Tiefgestellt

Formatiert: Tiefgestellt

In both summer and winter the maps of  $PM_{10}$ , and eBC in Fig. 2 exhibit a clear Northwest-to-Southeast structure with the cleanest sector being in the Northwest covering the coastal area of the North Sea, the BENELUX countries Belgium, the Netherlands, and Luxemburg, and Northwestern Germany. The strongest contrast between the cleanest Northwesterly and the most polluted Southeasterly map sectors is seen in the winter map of eBC. Highest average concentrations are measured in airmasses from the Southeastern half of the map, most strongly expressed in  $PM_{10}$  and eBC with maxima in a region leading from Southwest Poland through the Czech Republic, Slovakia, Austria, and former Yugoslavia to Northeastern Italy. The back trajectories in the Southeastern sector of the maps for  $PM_{10}$  and eBC point towards countries, in which the emissions of air pollution in the past 20 years developed very differently as compared to those in Western Europe. According to the European Environment Agency

(<https://www.eea.europa.eu/data-and-maps/dashboards/air-pollutant-emissions-data-viewer-2>)  
the latter parts of Western Europe experienced a strong and nearly monotonous decrease in  
emissions of PM<sub>10</sub> whereas the emissions in Poland, Czech Republic, Slovakia, Austria, former  
Yugoslavia, and Italy stayed nearly constant or even increased in recent years after the dramatic  
decreases in the course of the political developments of the 1990ies. The seasonal maps of the  
combustion derived SO<sub>2</sub> in Fig. S3 look very similar to the those of the particle-mass related  
maps of PM<sub>10</sub> and eBC, again the strongest NW/SE-contrast visible in winter.

374

## 375 5.2. Pollutant emissions and atmospheric processes

376

In Fig. 3 annual average emissions of PM<sub>10</sub>, BC, SO<sub>2</sub>, and NO<sub>x</sub> are mapped for 2009 according  
to the EDGAR emission database. Except for the absolute numbers the maps for SO<sub>2</sub>, and NO<sub>x</sub>  
look rather similar to those for particulate emissions. They all emphasize highly populated and  
industrialized emissions center. Beyond that the SO<sub>2</sub>-map accentuates individual large  
combustion sources such as conventional power plants. Whereas the strong emissions in  
Northern Italy are seen in the maps of PM<sub>10</sub>, BC, and NO<sub>x</sub> emissions in the countries in the  
Southeastern sector of the maps by no means reflect the high concentrations of particulate  
components seen in the immission maps of Figs. 1 and 2.

385

The seeming discrepancy between the immission maps in Figs. 1 and 2 and the emission  
maps of Fig. 3 can be resolved. For that purpose, the EDGAR-emissions of PM<sub>10</sub>, BC, SO<sub>2</sub>,  
and NO<sub>x</sub> along all 350593 hourly back trajectories to the four stations during the ten studied  
years were summed up. Then the sums were extrapolated back along each trajectory. In Fig.  
S4 10-year average maps of these extrapolated emission sums are displayed. As in Fig. 3 except  
for the absolute numbers there is a strong similarity between the four mapped component sums.  
Because of the integral nature of the mapped results one cannot expect the maps in Fig. S4 to

Gelöscht: the former countries

Formatiert: Tiefgestellt

Gelöscht: (Pruppacher and Klett, 1978)(Twomey, 1974)(Li et al., 2011)(Wichmann and Peters, 2000)(e.g., Wehner et al., 2007)In air masses from the extreme Southeastern sector of the map relatively low total number concentrations were measured. Even more so this holds for the relatively newly formed N<sub>10-26</sub> concentrations that exhibit a broad maximum in the Southwestern half of its map whereas N<sub>10-800</sub> has its maxima in a rather narrow band of air masses reaching from Switzerland through Southeastern Germany, Western Czech Republic to the former so called "Black Triangle" region near the Southeastern corner of Germany.

Current explanations of the new particle formation process (as indicated by N<sub>10-26</sub>) point towards photochemical processes that take place in plumes that contain sulfur dioxide (Größ et al., 2018). Several authors have stressed the possibility of particles to be formed in lofted layers, which are subsequently mixed to the ground (Platis, 2016), and/or in sulfur-rich plumes downstream of industrial point sources such as power plants (Junkermann and Hacker, 2018).

The trajectory extrapolated PM<sub>10</sub>-concentrations in Fig. 1 most strongly show the contrast between the relatively clean Northwest sector and the high concentrations in the Southeast sector of the maps.

Gelöscht: 2

Gelöscht: we collected

Gelöscht: PM<sub>10</sub>-

Formatiert: Tiefgestellt

Formatiert: Tiefgestellt

Gelöscht: corresponding

Gelöscht: (not shown)

Gelöscht: very

Gelöscht: Fig. 2 has little in common with the immission maps of Figs. 1.

427 locate correctly specific emission centers. However, they certainly indicate the map sectors  
428 from which the most substantial emissions could have reached the stations. As in Figs. 1 and  
429 2 the Southeastern sectors of the maps of integrated emissions most prominently show up.  
430 Interestingly, the maps in Fig. S4 also indicate the highly polluted region of Northwestern Italy  
431 (Diémoz et al., 2019a; Diémoz et al., 2019b). The emissions from the emission centers in  
432 Northwestern Europe are hardly discernible in Fig. S4. They do show up (most strongly in Fig.  
433 S4c for SO<sub>2</sub>-emission sums) as apparent emissions over the adjacent North Sea. We interpret  
434 the “misplaced” emissions over the North Sea as air mass transport from the North Sea via the  
435 emission region in the BENELUX countries to the receptor sites that was not compensated by  
436 other low pollution air transport from the North Sea to the stations that had not passed over the  
437 Northwestern European emission centers.

Formatiert: Tiefgestellt

Gelöscht: PM<sub>10</sub>-emissions are largely concentrated around major conurbations and highly populated and industrialized regions such as the German Ruhr area, and the BENELUX countries whereas highest PM<sub>10</sub>-concentrations were measured to some extent in air masses from the East and much more so in air masses from the Southeast.

Formatiert: Block

438  
439 Two major atmospheric processes will reduce the concentrations of emitted or in situ formed  
440 aerosol particles: dilution through mixing with cleaner air masses and wet scavenging through  
441 in-cloud and sub-cloud processes. As a tracer of the first of these two processes Fig. 4a gives  
442 the long-term average geographical distribution of trajectory derived wind speed over the study  
443 area. Highest average wind speeds and ensuing atmospheric mixing is seen over the major  
444 emission centers of Northwestern Germany, the BENELUX countries and adjacent seas  
445 whereas lowest wind speeds are seen over Northern Germany and the Southeastern neighbor  
446 countries. The long-term average geographical distribution of precipitation as taken by  
447 HYSPLIT from the GDAS meteorological fields in Fig. 4b corroborates the results about  
448 atmospheric cleaning processes indicated in Fig. 4a. The small absolute numbers in Fig. 4b are  
449 due to the episodic nature of precipitation: most of the time it does not rain or snow. The blue  
450 crescent reaching from the North Sea through the BENELUX countries, Eastern France,  
451 Switzerland and the alpine region exhibits maximum precipitation values while Southern and  
452 Eastern Germany with the adjoining countries to the East and Southeast show minimum

Gelöscht: 3a

Gelöscht: 3b

Gelöscht: 3a

Gelöscht: 3b



463 precipitation values. Thus, in the long term we expect much of the high Western European  
464 emissions to be scavenged to a substantially by wet processes. In addition, air masses arriving  
465 from Western and Northwestern directions at the stations usually cross the Western European  
466 emission centers with much lower pollution burdens than air masses coming from the polluted  
467 countries of Southeastern Europe arriving at the corresponding map borders (cf. Fig. PM<sub>10</sub> —  
468 36th maximum daily average value in  $\mu\text{g m}^{-3}$ , 2005 in EEA, 2009).

Gelöscht: three

### 470 **5.3. Immission trends for air from specific source regions**

471  
472 As mentioned in the introduction, the pollutant emissions reported by the European and national  
473 Environment Agencies represent a synthesis of known pollutant sources combined with  
474 assumed emission factors. These emissions are typically used as input for air quality modelling  
475 and subsequent assessment, as well as for trend analyses. However, it remains unclear to what  
476 extent these reported emissions are realistic, and whether their trends represent the trend in true  
477 emissions. Here, we attempt to assess spatially-resolved trends in real particulate emissions by  
478 an analysis of measured concentrations (immissions) in air masses travelling over source-  
479 specific regions.

480  
481 To test our method, we selected two pronounced source regions in Europe, located within  
482 1000 km distance from our observation sites. These regions were defined by emission hotspot  
483 regions that can be seen in the EDGAR emission maps in Fig. 3a-b and comprise: Region A  
484 (Be-NL-NRW; comprising most of Belgium, southern parts of the Netherlands, and much of  
485 the German state North Rhine-Westphalia) and Region B (CZ-PL-SK; comprising the central  
486 parts of the Czech Republic, southern parts of Poland, and adjacent areas of Slovakia.)  
487 According to the European Environment Agency (EEA) these are regions, where reported

particulate emissions have developed differently during the past 10 years. Our goal is to verify this through an analysis of real atmospheric observations over this period. Temporal trends were computed using the customized Sen–Theil trend estimator (Sen, 1968; Theil, 1992). The Sen–Theil estimator is the median of many slopes calculated in a continuous or non-continuous time series, with its robustness against outliers being one of its main assets. For the detailed description of this trend estimator we refer to Sun et al. (2020), Section 2.3.1. Here we computed the Sen–Theil estimator for hourly observation data at stations ME, NG, and WA. Subsets of back trajectories were selected that spent at least 1, 3, 6, or 12 hours over the source regions A and B. Depending on that criterion, different sub-sets were analyzed. The difference in median eBC mass concentration between air masses arriving from source region A and B is obvious, as could already be determined in the corresponding immission maps (Fig. 2c-d). As we learned from Sect. 5.2 these immission maps are strongly influenced by the different meteorological conditions governing atmospheric dispersion in different wind direction, so that these values allow no direct conclusion on the strength of emission sources located upwind.

We analyzed the temporal trends in eBC over the period 2009-2018 for the subsets belonging to Regions A and B – assuming that these systematic differences in meteorological conditions should even out over such long observation periods. Table 2 shows that the Sen–Theil slope estimator for Region A is between -7.6 % and -5.1 % for the three observation sites and the requirement of a back trajectory to have spent at least 6 hours over Region A. For region B, the corresponding Sen–Theil slope estimators are between -4.0 % and -2.7 % for the observation sites. As we can read from these results, the annual decrease in eBC is more pronounced for air masses that have travelled over Region A.

Between 2009 and 2017 for the EU member states of Belgium, the Netherlands, Germany, the Czech Republic, Poland, and Slovakia the annual rates of decrease in reported emissions were between -4.9 and -6.1 % for the first three countries, and between +0.5 and -2.8% for the latter three (<https://www.eea.europa.eu/data-and-maps/dashboards/air-pollutant-emissions-data-viewer-2>). As compiled in Table 2 these reported trends are largely consistent with the rates of change derived from our eBC immission trends. Although we need to keep in mind that the six nation states only partially contribute to our regions A and B, it seems valid to conclude that BC emissions in region A indeed decreased more rapidly in the past decade compared to region B. Our approach seems able to differentiate between concentrations trends in air masses that have passed over rather different source regions. This might represent a step towards the assessment of changes in real-world emissions allocated in specific source regions over multi-annual periods.

#### 5.4. Comparison of immission and emission trends

Besides the map comparison a second approach was used to connect emission data with the measured aerosol time series. Along each of the hourly back trajectories the emissions according to the EDGAR database were summed up. Then monthly medians of the emission sums and the measured parameters were formed. The EDGAR database reports annual average emissions. PM<sub>10</sub>, black carbon and other combustion related air pollutants show substantial annual variations with high winter and low summer values at non-urban sites (e.g., Heintzenberg and Bussemer, 2000). In emission modeling the temporal variation of annually reported emissions is considered by disaggregating the annual values with monthly, weekly and daily factors (Matthias et al., 2018). For the time-resolved comparison of PM<sub>10</sub> and BC-emissions with PM<sub>10</sub> and eBC-concentrations at the GUAN-sites monthly medians of PM<sub>10</sub> and eBC-values at the stations were formed and plotted in Fig. 5. We expected both, seasonal

Gelöscht: →

Gelöscht: 4

[1] verschoben (Einfügung)

Gelöscht:

543 variations and a long-term trend in the emissions. For  $M$  hours per month of measured  
 544 components at the four stations the annual average EDGAR-emissions  $E_{PM10}$ ,  $E_{BC}$ ,  $E_{SO2}$ , and  
 545  $E_{NOx}$  were summed up along the 121 trajectory steps leading to the stations. Then monthly  
 546 medians  $\tilde{E}_{i=1,4}$  were formed according to Eq. 1 (exemplified for BC). Medians were chosen to  
 547 reduce the effect of outliers due to local emission and scavenging events.

$$549 \quad \tilde{E}_{BC} = \text{Median}(\sum_{n=1}^{121} E_{BC})_{m=1,M} \quad \text{Eq. 1}$$

550  
 551 The monthly median emission sums  $\tilde{E}_{i=1,4}$  were modified with a monthly ( $f_m$ ) and an annual  
 552 factor ( $g_y$ ) in order to simulate respective median monthly measured concentrations taken over  
 553 all stations. Thus, for each component 12 monthly and 10 annual trend factors determined the  
 554 agreement of modified summed emissions and measured concentrations. As objective or utility  
 555 function  $\chi^2$  the sum of squared deviations between annually and monthly modified emission  
 556 sums and monthly median measured concentrations was formed taken over the 120 months of  
 557 the present study (exemplified for BC in Eq. 2).

$$559 \quad \chi_{BC}^2 = \sum_{j=1}^{120} (f_{m=1,12} \cdot g_{y=1,10} \cdot \tilde{E}_{BC} - e_{BC})^2 \quad \text{Eq. 2}$$

560  
 561  $\chi^2$  was minimized with a Generalized Reduced Gradient (GRG) solver (Lasdon et al., 1978)  
 562 that optimized the 12 monthly and 10 annual factors for each of the four measured components.  
 563 We used Excel's<sup>®</sup> implementation of the GRG-solver procedure for the optimization. After  
 564 optimizing month and trend factors the average relative deviation between emission-simulated  
 565 and measured monthly median curves is 14%, 21%, 25%, and 18% for PM<sub>10</sub>, eBC, SO<sub>2</sub>, and  
 566 NO<sub>x</sub>, and respectively. The optimized monthly median emission sums for all four parameters  
 567 are displayed in Fig. 5 together with the measured monthly median concentrations.

Formatiert: Schriftart: Kursiv

Formatiert: Schriftart: Kursiv

Formatiert: Schriftart: Kursiv, Tiefgestellt

Formatiert: Schriftart: Kursiv

Formatiert: Schriftart: Kursiv, Tiefgestellt

Formatiert: Schriftart: Kursiv

Formatiert: Schriftart: Kursiv, Tiefgestellt

Formatiert: Schriftart: Kursiv

Gelöscht: calculated

Formatiert: Schriftart: Kursiv, Tiefgestellt

Gelöscht: PM<sub>10</sub>, BC, SO<sub>2</sub>, and NO<sub>x</sub>-emissions were summed up along the hourly back-trajectories to the stations and monthly medians of these sums

Formatiert: Schriftart: Kursiv, Tiefgestellt

Formatiert: Schriftart: Kursiv

Formatiert: Schriftart: Kursiv, Tiefgestellt

Formatiert: Schriftart: Kursiv, Tiefgestellt

Formatiert: Schriftart: Kursiv

Formatiert: Schriftart: Kursiv, Tiefgestellt

Formatiert: Schriftart: Kursiv

[1] nach oben verschoben: We expected both, seasonal variations and a long-term trend in the emissions.

Gelöscht: In order to optimize the

Formatiert: Tabstopps: 15 cm, Links

Gelöscht: we used Excel's<sup>®</sup>

Formatiert: Rechtschreibung und Grammatik prüfen

Gelöscht: The GRG-solver minimizes the average absolute deviation between the two monthly time series by varying ten annual and 12 monthly adjustment factors at the summed emissions.

Gelöscht: The

Gelöscht: was repeated for a fit of the trajectory-summed emissions of PM<sub>10</sub>, BC, SO<sub>2</sub>, and NO<sub>x</sub> with the respective measured time series

Gelöscht: ation of

Gelöscht: trends and

Gelöscht: the two

Gelöscht: are

Gelöscht: 4

589

590 A ten-year trend in emissions of PM<sub>10</sub>, BC, SO<sub>2</sub>, and NO<sub>x</sub>, and average monthly factors for  
591 the respective parameters are the two essential results derived from the optimization approach.

592 The ten-year trends relative to 2009 are collected in Fig. 6. Annual averages of the relative  
593 differences between the monthly median measured parameters and the corresponding emission  
594 derived parameters were formed and applied to the GUAN-trend values displayed in Fig. 6.  
595 The resulting error bars on the trends serve as estimates of the uncertainties of the optimization  
596 approach. The general trend in Fig. 6 is downward to minima between 30 and 70% of the 2009  
597 values in 2016/17 after which all parameters exhibit increases, most strongly PM<sub>10</sub>. SO<sub>2</sub> shows  
598 the strongest decrease whereas PM<sub>10</sub> and NO<sub>x</sub>-emissions diminished the least. In 2010/2011  
599 the trend curves of PM<sub>10</sub> and NO<sub>x</sub> in Fig. 6 show a slight increase that can be linked to a recovery  
600 of economic activity after the world-wide financial and economic crisis during the period 2007-  
601 2009. The increase in PM<sub>10</sub> is also visible in the trend curves relative to

602 2005 published by the German Environment Agency

603 ([https://www.umweltbundesamt.de/daten/luft/luftschadstoff-emissionen-in-](https://www.umweltbundesamt.de/daten/luft/luftschadstoff-emissionen-in-deutschland/emissionen-prioritaerer-luftschadstoffe)

604 [deutschland/emissionen-prioritaerer-luftschadstoffe](https://www.umweltbundesamt.de/daten/luft/luftschadstoff-emissionen-in-deutschland/emissionen-prioritaerer-luftschadstoffe)).

605

606 The results of two comparisons of our trends with data reported by the German and European  
607 Environment Agencies are added to Fig. 6. In general, the trends reported by the German  
608 Environment Agency for all German emissions exhibit weaker reductions than the results of  
609 the present study. Only for PM<sub>10</sub> in 2011 and 2013 the present study yields higher values than  
610 GEA. We note that primary PM<sub>10</sub>-emissions may have substantial contributions from wind  
611 erosion of agricultural soils (Panagos et al., 2015) that are not incorporated in present  
612 anthropogenic inventories. SO<sub>2</sub> exhibits the strongest trend discrepancies with much stronger  
613 reductions in trend of the present study as compared to GEA results. As Germany has been  
614 reducing SO<sub>2</sub> emissions systematically since the nineteen eighties one would not expect any

Gelöscht: 5

Gelöscht: in 2010

Gelöscht: and can be linked to a recovery of economic activity after the world-wide financial and economic crisis during 2007-2009

Gelöscht: 5

Formatiert: Rechtschreibung und Grammatik prüfen

621 further strong trends during the time period of the present study. As other studies have  
622 demonstrated before, (e.g., van Pinxteren et al., 2019), the maps in Fig. 1 indicate the possibility  
623 of imported pollution, in particular from the Southeast. Consequently, we searched for similar  
624 trends in emission data reported by EEA for neighboring countries until 2017 directly West,  
625 South, and East of Germany, going in the East all the way to Romania. Excel's solver optimized  
626 combinations of the EEA-trends for Germany and neighboring countries in order to fit the  
627 trends derived in the present study. The solver did not choose German trends for any of the  
628 four parameters PM<sub>10</sub>, BC, SO<sub>2</sub>, and NO<sub>x</sub>. For PM<sub>10</sub> a combination of emission trends for the  
629 BENELUX countries and France was optimum, albeit without being able to simulate the  
630 relative maxima in 2011 and 2013 and the minimum around 2016. For BC the emission trend  
631 for the BENELUX countries came closest to the trend of the present study. For SO<sub>2</sub> mostly  
632 emissions in Romania with minor contributions from French and BENELUX trends simulated  
633 the trends observed over Germany best. NO<sub>x</sub>-trends were best simulated by emissions over the  
634 Czech and Slovakian countries. Emissions trends over Switzerland, Austria, Hungary and  
635 Poland were not utilized by the solver. All simulated trends are displayed as curves EEA in  
636 Fig. 6. We do not claim that these simulated trends numerically correspond to imported  
637 pollution over Germany. However, the good fit of SO<sub>2</sub>-trend with emissions over Romania  
638 corroborates our finding of pollution import from Southeastern Europe to Northeastern  
639 Germany while the development of BC appears to follow better emission trends over Western  
640 neighbor countries than over Germany.

642 ▼ Sun et al., (2020) investigated trends of size resolved number and eBC mass concentrations  
643 at 16 observational sites in Germany from 2009 to 2018 including the three GUAN-sites of the  
644 present study. Based on monthly median time series they report average decreases for ME,  
645 NG, and WA of -5.5%, -6.1, and -3.9%, respectively. The corresponding result for eBC of the

Gelöscht: 5

Gelöscht: (2019a)

Gelöscht: particle

present study is -4.6%, albeit with a high variability (cf. Fig. 6) of 20 percent units expressed in terms of a standard deviation.

Over the polluted continent the particle-number based parameter  $N_{10-800}$  is largely secondary in nature, i.e., its concentrations are controlled by atmospheric constituents and processes. Thus, there is no primary emission data base with which a similar trend analysis as with  $PM_{10}$ ,  $BC$ ,  $SO_2$ , and  $NO_x$  could be attempted. Instead we chose the 10-year Grand Averages (GA) averages taken over the whole time period of the present study as references from the deviations of annual averages are discussed. Sun et al. (2020) report very minor trends (between -3.5% and 0.1%) for  $N_{20-800}$  at the three GUAN stations of the present study. The 10-year interannual variation of our  $N_{10-800}$  in Fig. 7a) bears out why only a minor trend if any can be expected. For the first four years the annual averages are substantially higher than average. Then annual values decrease down to a minimum in the years 2016/17 before they increase again to a level slightly above the 10-year average.

In Figs 7b-d) annual deviations from the respective GAs are displayed that can be connected to the 10-year course of  $N_{10-800}$ . Ozone concentrations averaged over the data from the three GUAN stations can be interpreted as an indicator for photochemical activity that also controls NPF. The annual deviations of  $O_3$  in Fig. 7b) follow rather closely those of  $N_{10-800}$ . In Figs 7c) and d) annual deviations of ambient temperature and precipitation rates are displayed that have been averaged over the meteorological data along the back trajectories leading to the four stations. For the temperature an averaging period of 120 trajectory hours yielded the highest (negative) correlation with  $N_{10-800}$  of  $r = -0.8$ . After a dip in 2009 annual average trajectory temperatures to a maximum in 2016 before returning to near average in 2018. For the precipitation rates along the trajectories the highest (negative) correlation with  $N_{10-800}$  was found with an averaging period of three days ( $r = -0.6$ ) before arrival at the stations. The results

displayed in Figs 7c) and d) illustrate the complexity of processes and conditions controlling atmospheric particle number concentrations. On one hand, a scavenging effect of precipitation can be used as argument for the high values of  $N_{10-800}$  in the years 2010-2013 and the low values in the years 2014 through 2018. On the other hand, lower annual temperatures during years of relatively high  $N_{10-800}$  and higher than GA-temperatures during years of relatively high  $N_{10-800}$  are harder to interpret. Possibly the nucleation of condensable vapors is furthered by lower air temperatures upwind of the stations.

An important result of trend analysis are the average monthly factors disaggregating the annual emissions. In general the summer minima of the month factors determined in the present study are broader than the curve given by Matthias et al., (2018) for combustion emissions. The decrease of the month factor of  $PM_{10}$ , BC, and  $NO_x$  in December and the late winter maxima of  $PM_{10}$  and  $SO_2$  are not reflected in the Matthias et al., (2018) results. Interestingly, both  $PM_{10}$  and  $SO_2$  show a minor secondary peak in June. As an example of the seasonal variability of eBC within an urban source region we averaged the relative annual variation of eBC-concentrations at the station Leipzig Eisenbahnstraße (plotted as curve L-EBS in Fig. 8) exhibiting a smaller seasonal swing than all other curves. The curve for  $PM_{10}$  comes closest to that for L-EBS, probably because of agricultural non-combustion emissions in summer.

In general the downward trends in particulate parameters determined in the present study are similar to temporal trends of particle number and black carbon mass concentrations at 16 observational sites in Germany from 2009 to 2018 (Sun et al., 2020). The long-term emission-decrease of  $PM_{10}$  as determined in the present study from 2009 to 2018 is smaller than the corresponding number published by the EEA as average over all 28 EU member-states but similar to the figures published by GEA until 2017 (cf. Table 2). For BC,  $SO_2$ , and  $NO_x$  the present study yields substantially stronger emission-reductions than both GEA and EEA. These

Gelöscht: The second

Gelöscht: our optimized

Gelöscht: 6



705 findings are emphasized when considering 2017 as endpoint of the trend calculation (cf. Table  
706 2) at and after which our study shows consistent emission increases of all studied parameters.  
707 Comparing the calculated trends with emission trends in neighboring countries as published by  
708 the European Environment Agency supports the explanation that the observed trends are to  
709 some extent due to changes in imported air masses. Most strongly this holds for SO<sub>2</sub>, the trend  
710 of which follows that of Romanian emissions rather well.

711

712 The last issue we take up in this discussion concerns the frequent residual difference between  
713 measured and emission-simulated time series. In Fig. 5, e.g., in most winters there are months  
714 when optimized BC-emissions remain substantially lower than the measured monthly medians  
715 of eBC. Some information can be gleaned from the “Großwetterlagen”, (GWL), representing  
716 29 classifications of large scale weather types after Hess and Brezowsky for Central Europe,  
717 (Gerstengarbe and Werner, 1993), provided by the German Weather service for each day  
718 (<http://www.dwd.de/DE/leistungen/grosswetterlage/grosswetterlage.html>). During the winter  
719 months with the strongest difference between measured and simulated time series the  
720 probabilities of high-pressure systems over Fennoscandia with south-to-southeasterly flow to  
721 the four stations is substantially higher than the respective probabilities averaged over the whole  
722 ten-year period of the study. This GWL-information is consistent with the back trajectories  
723 during the high pollution winter months coming predominantly from the southeasterly sector  
724 of the map. While the classified large-scale weather situation with weak dilution of pollution  
725 during the winter months is conducive of high particulate concentrations at the receptor sites it  
726 does not explain the discrepancy. In principle our simplistic approach of accumulating  
727 emissions along back trajectories may be flawed during certain weather situations. However,  
728 an alternative explanation could be that the emissions inventories over Eastern and Southeastern  
729 Europe in the EDGAR database are somewhat lower than the real emissions.

730

Gelöscht: 4

Formatiert: Englisch (USA)

## 6 Summary and conclusions

Ten years of hourly aerosol and gas data at three stations of the German Ultrafine Aerosol Network GUAN and one station of the Saxonian Environment Agency have been combined with hourly back trajectories to the stations and emission inventories. Measured PM<sub>10</sub>, particle number concentrations between 10 and 800 nm, and equivalent black carbon were extrapolated along the trajectories. This process yielded what we termed immission maps of these aerosol parameters over Germany. They reflect aerosol emissions modified with atmospheric processes along the air mass transport between sources and the four receptor sites at which potential effects of the particulate air pollution would be realized.

The ten-year average immission maps do not simply show the distribution of pollution sources upwind of the receptor sites. The comparison with emission data based on the European EDGAR emission database shows that strong Western European emission centers do not dominate the downwind concentrations because their emissions often are reduced by wet scavenging and dilution processes on the way to the receptor area. Maps of average precipitation and wind as they occurred along the trajectories illustrate these processes. In the receptor region mass related aerosol parameters such as PM<sub>10</sub>, equivalent black carbon, and to some extent also the particle number concentration instead is rather controlled by emissions from Eastern and Southeastern Europe from which pollution transport often occurs under dryer meteorological conditions in continental high-pressure air masses. This finding corresponds to the air mass results derived for the sub-micrometer particle number size distribution by Birmili et al., (2001), by Engler et al., (2007) for the size distribution of non-volatile particles, by Ma et al., (2014) for optical particle properties all evaluated at the station Melpitz, and by van

Gelöscht: maps

Gelöscht: necessarily

Gelöscht: on average

Gelöscht: illuminated

Formatiert: Rechtschreibung und Grammatik prüfen

Formatiert: Rechtschreibung und Grammatik prüfen

Pinxteren et al., (2019) for transboundary transport of PM<sub>10</sub> to ten stations in Eastern Germany from neighboring countries. Newly formed particles on the other hand are found in air masses from a broad belt reaching from Burgundy to the Western Czech Republic and Southern Poland, a region with high photochemical activity in summer that is affected by emissions in Northern Italy.

**Gelöscht:** geographical sector

**Gelöscht:** Southern Germany to the BENELUX countries

**Gelöscht:**

**Gelöscht:** which we explain with gaseous particle precursors being transported with little wet scavenging from this region

Annual EDGAR emissions for 2009 of PM<sub>10</sub>, BC, SO<sub>2</sub>, and NO<sub>x</sub>, were accumulated along each trajectory and compared the calculated emission sums with the corresponding measured time series on a monthly basis. With a generalized reduced gradient solver the agreement of each pair of monthly time series e.g., measured eBC and BC-emissions was optimized by letting the solver determine both monthly emission factors disaggregating the annual EDGAR emission fields and adjusting the emissions with annual factors modifying the 2009-fields.

**Gelöscht:** s a test of the justifiability of our trajectory approach we accumulated the a

**Gelöscht:** the

**Gelöscht:** (GRG)

**Gelöscht:** provided by EXCEL® we optimized

**Gelöscht:** on

Relative to 2009 the annual averages of the analyzed air pollutants were lower in 2018 by values between 6% for PM<sub>10</sub> and 60% for SO<sub>2</sub>. In general, the ten-year reductions determined of the present study were stronger than those reported by the German and the European Environmental Agencies. N<sub>10-800</sub> exhibited substantial interannual variability but no net decrease over the ten studied years.

**Formatiert:** Tiefgestellt

**Formatiert:** Tiefgestellt

**Formatiert:** Tiefgestellt

The validity of the present approach of connecting immission and emission of particulate pollution was tested by calculating temporal changes of eBC for subsets of back trajectories passing over two separate prominent emission regions, region A to the Northwest and B to the Southeast of the measuring stations. Consistent with reported emission data the calculated immission decreases over region A are significantly stronger than over region B.

Compared to published emission monthly factors by Matthias et al., (2018) the present approach yielded broader summer minima that were partly displaced from the midsummer

798 positions given by Matthias et al., (2018). As an aside we note that during the winter months  
799 with extremely high particulate pollution the emissions accumulated along back trajectories  
800 often are substantially lower than the measured concentrations which raises the question of the  
801 validity of the emission figures in Eastern and Southeastern European source regions.

802

803 There are clear limits in the methodology of the present study. Air mass trajectories have  
804 inherent uncertainties increasing with their distance travelled (Stohl, 1998). Meteorological  
805 processes affecting the aerosol during air mass transport are only considered rather coarsely  
806 whereas aerosol dynamics are not considered at all. Possible future improvements concern  
807 ensemble trajectories with higher resolution, better meteorological information along the  
808 trajectories e.g., radar-derived precipitation as used in Heintzenberg et al., (2018), more  
809 comprehensive emission inventories with higher spatiotemporal resolution and higher numbers  
810 of analyzed stations.

811

812 Acknowledgements

813

814 This work was accomplished in the framework of the project ACTRIS-2 (Aerosols, Clouds,  
815 and Trace gases Research InfraStructure) under the European Union—Research Infrastructure  
816 Action in the frame of the H2020 program for “Integrating and opening existing national and  
817 regional research infrastructures of European interest” under Grant Agreement N654109,  
818 (H2020—Horizon 2020). Additionally, we acknowledge the WCCAP (World Calibration  
819 Centre for Aerosol Physics) as part of the WMO-GAW program base-funded by the German  
820 Federal Environmental Agency (UBA). Continuous aerosol measurements as well as data  
821 processing at Melpitz, Waldhof and Neuglobsow were supported by the German Federal  
822 Environment Agency Grants F&E 370343200 (German title: “Erfassung der Zahl feiner und  
823 ultrafeiner Partikel in der Außenluft”), and F&E 371143232 (German title: “Trendanalysen

Formatiert: Rechtschreibung und Grammatik prüfen

Gelöscht: involved

Formatiert: Englisch (USA)

825 gesundheitsgefährdender Fein-und Ultrafeinstaubfraktionen unter Nutzung der im German  
826 Ultrafine Aerosol Network (GUAN) ermittelten Immissionsdaten durch Fortführung und  
827 Interpretation der Messreihen). We gratefully acknowledge receiving the emission data set  
828 from European emission data base for global atmospheric research (EDGAR). We  
829 acknowledge technical support by Annette Pausch of the Saxon State Office for Environment,  
830 Agriculture and Geology at the Collmberg station, Achim Grüner und René Rabe (TROPOS)  
831 at the Melpitz station, by Olaf Bath (GEA) at the Neuglobsow station, and Andreas Schwerin  
832 (GEA) at the Waldhof station. Fabian Senf compiled the “Großwetterlagen” for the present  
833 study. We are most grateful for the ideas provided by Peter Winkler in the interpretation of  
834 data.

**Gelöscht:** support given

835

837 Literature

838

839 Anderson, J. O., Thundiyil, J. G., and Stolbach, A.: Clearing the air: a review of the effects of  
840 particulate matter air pollution on human health, *J Med Toxicol*, 8, 166-175,  
841 10.1007/s13181-011-0203-1, 2012.

842 Beekmann, M., Prévôt, A. S. H., Drewnick, F., Sciare, J., Pandis, S. N., Denier van der Gon,  
843 H. A. C., Crippa, M., Freutel, F., Poulain, L., Gherzi, V., Rodriguez, E., Beirle, S.,  
844 Zotter, P., von der Weiden-Reinmüller, S. L., Bressi, M., Fountoukis, C., Petetin, H.,  
845 Szidat, S., Schneider, J., Rosso, A., El Haddad, I., Megaritis, A., Zhang, Q. J., Michoud,  
846 V., Slowik, J. G., Moukhtar, S., Kolmonen, P., Stohl, A., Eckhardt, S., Borbon, A., Gros,  
847 V., Marchand, N., Jaffrezo, J. L., Schwarzenboeck, A., Colomb, A., Wiedensohler, A.,  
848 Borrmann, S., Lawrence, M., Baklanov, A., and Baltensperger, U.: In situ, satellite  
849 measurement and model evidence on the dominant regional contribution to fine  
850 particulate matter levels in the Paris megacity, *Atmos. Chem. Phys.*, 15, 9577-9591,  
851 10.5194/acp-15-9577-2015, 2015.

852 Birmili, W., Wiedensohler, A., Heintzenberg, J., and Lehmann, K.: Atmospheric particle  
853 number size distribution in Central Europe: Statistical relations to air masses and  
854 meteorology, *J. Geophys. Res.*, 106, 32005-32018, 2001.

855 Birmili, W., Weinhold, K., Merkel, M., Rasch, F., Sonntag, A., Wiedensohler, A., Bastian, S.,  
856 Schladitz, A., Löschau, G., Cyrys, J., Pitz, M., Gu, J., Kusch, T., Flentje, H., Quass, U.,  
857 Kaminski, H., Kuhlbusch, T. A. J., Meinhardt, F., Schwerin, A., Bath, O., Ries, L.,  
858 Wirtz, K., and Fiebig, M.: Long-term observations of tropospheric particle number size  
859 distributions and equivalent black carbon mass concentrations in the German Ultrafine  
860 Aerosol Network (GUAN), *Earth Syst. Sci. Data*, 8, 355-382, doi:10.5194/essd-8-355-  
861 2016, 2016.

Formatiert: Block, Einzug: Links: 0 cm, Hängend: 1.25  
cm, Zeilenabstand: Doppelt

862 Bond, T. C., Doherty, S. J., Fahey, D. W., Forster, P. M., Berntsen, T., DeAngelo, B. J., Flanner,  
 863 M. G., Ghan, S., Kärcher, B., Koch, D., Kinne, S., Kondo, Y., Quinn, P. K., Sarofim,  
 864 M. C., Schultz, M. G., Schulz, M., Venkataraman, C., Zhang, H., Zhang, S., Bellouin,  
 865 N., Guttikunda, S. K., Hopke, P. K., Jacobson, M. Z., Kaiser, J. W., Klimont, Z.,  
 866 Lohmann, U., Schwarz, J. P., Shindell, D., Storelvmo, T., Warren, S. G., and Zender,  
 867 C. S.: Bounding the role of black carbon in the climate system: A scientific assessment,  
 868 *J. Geophys. Res.*, doi: 10.1002/jgrd.50171, [10.1002/jgrd.50171](https://doi.org/10.1002/jgrd.50171), 2013.

869 Cass, G. R., and McRae, G. J.: Source-receptor reconciliation of routine air monitoring data for  
 870 trace metals: An emission inventory assisted approach, *Environ. Sci. Technol.*, 17, 129-  
 871 139, 1983.

872 Charron, A., Birmili, W., and Harrison, R. M.: Fingerprinting particle origins according to their  
 873 size distribution at a UK rural site, *J. Geophys. Res.*, 113, D07202,  
 874 doi:10.1029/2007JD008562, 2008.

875 Crippa, M., Guizzardi, D., Muntean, M., Schaaf, E., Dentener, F., van Aardenne, J. A., Monni,  
 876 S., Doering, U., Olivier, J. G. J., Pagliari, V., and Janssens-Maenhout, G.: Gridded  
 877 emissions of air pollutants for the period 1970–2012 within EDGAR v4.3.2, *Earth Syst.*  
 878 *Sci. Data*, 10, 1987-2013, [10.5194/essd-10-1987-2018](https://doi.org/10.5194/essd-10-1987-2018), 2018.

879 Diémoz, H., Barnaba, F., Magri, T., Pession, G., Dionisi, D., Pittavino, S., Tombolato, I. K. F.,  
 880 Campanelli, M., Della Ceca, L. S., Hervo, M., Di Liberto, L., Ferrero, L., and Gobbi, G.  
 881 P.: Transport of Po Valley aerosol pollution to the northwestern Alps – Part 1:  
 882 Phenomenology, *Atmos. Chem. Phys.*, 19, 3065-3095, [10.5194/acp-19-3065-2019](https://doi.org/10.5194/acp-19-3065-2019),  
 883 2019a.

884 Diémoz, H., Gobbi, G. P., Magri, T., Pession, G., Pittavino, S., Tombolato, I. K. F., Campanelli,  
 885 M., and Barnaba, F.: Transport of Po Valley aerosol pollution to the northwestern Alps  
 886 – Part 2: Long-term impact on air quality, *Atmos. Chem. Phys.*, 19, 10129-10160,  
 887 [10.5194/acp-19-10129-2019](https://doi.org/10.5194/acp-19-10129-2019), 2019b.

888 Draxler, R., and Hess, G.: An overview of the HYSPLIT\_4 modeling system for trajectories,  
889 dispersion, and deposition, *Austr. Meteor. Mag.*, 47, 295-308, 1998.

890 EEA: Spatial assessment of PM<sub>10</sub> and ozone concentrations in Europe (2005), European  
891 Environmental Agency, Copenhagen, Denmark, 52 pp, 2009.

892 Eliassen, A.: The OECD Study of Long Range Transport of Air Pollutants: Long Range  
893 Transport Modelling, *Atmos. Environ.*, 12, 479-487, 1978.

894 Engler, C., Rose, D., Wehner, B., Wiedensohler, A., Brüggemann, E., Gnauk, T., Spindler, G.,  
895 Tuch, T., and Birmili, W.: Size distributions of non-volatile particle residuals (Dp<800  
896 nm) at a rural site in Germany and relation to air mass origin, *Atmos. Chem. Phys.*, 7,  
897 5785-5802, 10.5194/acp-7-5785-2007, 2007.

898 Friedlander, S. K.: Chemical element balances and identification of air pollution sources, *Env.*  
899 *Sci. & Technol.*, 7, 235-240, 10.1021/es60075a005, 1973.

900 Gerstengarbe, F.-W., and Werner, P. C.: Katalog der Grosswetterlagen Europas nach Paul Hess  
901 und Helmut Brezowski 1881-1992, 4., vollständ. neu bearb. Aufl., Deutscher  
902 Wetterdienst, Offenbach, Germany, 1993.

903 Heintzenberg, J., and Bussemer, M.: Development and application of a spectral light absorption  
904 photometer for aerosol and hydrosol samples, *J. Aerosol Sci.*, 31, 801-812, 2000.

905 Heintzenberg, J., Birmili, W., Seifert, P., Panov, A., Chi, X., and Andreae, M. O.: Mapping the  
906 aerosol over Eurasia from the Zotino Tall Tower (ZOTTO), *Tellus B*, 65,  
907 doi:<http://dx.doi.org/10.3402/tellusb.v3465i3400.20062>, 2013.

908 Heintzenberg, J., Leck, C., and Tunved, P.: Potential source regions and processes of aerosol  
909 in the summer Arctic, *Atmos. Chem. Phys.*, 15, 6487-6502, 10.5194/acp-15-6487-2015,  
910 2015.

911 Heintzenberg, J., Senf, F., Birmili, W., and Wiedensohler, A.: Aerosol connections between  
912 distant continental stations, *Atmos. Environ.*, 190, 349-358, 2018.



913 Hůnová, I.: Ambient air quality for the territory of the Czech Republic in 1996–1999 expressed  
 914 by three essential factors, *Sci. Total Environ.*, 303, 245-251,  
 915 [https://doi.org/10.1016/S0048-9697\(02\)00493-X](https://doi.org/10.1016/S0048-9697(02)00493-X), 2003.

916 Hůnová, I., and Bäumelt, V.: Observation-based trends in ambient ozone in the Czech Republic  
 917 over the past two decades, *Atmos. Environ.*, 172, 157-167,  
 918 <https://doi.org/10.1016/j.atmosenv.2017.10.039>, 2018.

919 Kanamitsu, M.: Description of the NMC Global Data Assimilation and Forecast System, *Wea.*  
 920 *Forecasting*, 4, 335-342, 10.1175/1520-0434(1989)004<0335:DOTNGD>2.0.CO;2,  
 921 1989.

922 Klimont, Z., Kupiainen, K., Heyes, C., Purohit, P., Cofala, J., Rafaj, P., Borken-Kleefeld, J.,  
 923 and Schöpp, W.: Global anthropogenic emissions of particulate matter including black  
 924 carbon, *Atmos. Chem. Phys.*, 17, 8681-8723, 10.5194/acp-17-8681-2017, 2017.

925 Krige, D. G.: A statistical approach to some basic mine valuation problems on the  
 926 Witwatersrand, *J. Chem. Metall. Min. Soc. S. Afr.*, December, 119-159, 1951.

927 Kuenen, J. J. P., Visschedijk, A. J. H., Jozwicka, M., and Denier van der Gon, H. A. C.: TNO-  
 928 MACC-II emission inventory; a multi-year (2003 - 2009) consistent high-resolution  
 929 European emission inventory for air quality modelling, *Atmos. Chem. Phys.*, 14, 10963-  
 930 10976, 10.5194/acp-14-10963-2014, 2014.

931 Kulmala, M., Vehkamäki, H., Petäjä, T., Dal Maso, M., Lauri, A., Kerminen, V.-M., Birmili,  
 932 W., and McMurry, P. H.: Formation and growth rates of ultrafine atmospheric particles:  
 933 a review of observations, *J. Aerosol Sci.*, 35, 143-176, 2004.

934 Lasdon, L. S., Waren, A. D., Jain, A., and Ratner, M.: Design and Testing of a Generalized  
 935 Reduced Gradient Code for Nonlinear Programming, *ACM Trans. Math. Softw.*, 4, 34-  
 936 50, 10.1145/355769.355773, 1978.

937 Lavanchy, V. M. H., Gäggeler, H. W., Schotterer, U., Schwikowski, M., and Baltensperger, U.:  
 938 Historical record of carbonaceous particle concentrations from a European high-alpine  
 939 glacier (Colle Gnifetti, Switzerland), *J. Geophys. Res.*, 104, 21227-21236, 1999.  
 940 Leibensperger, E. M., Mickley, L. J., Jacob, D. J., Chen, W. T., Seinfeld, J. H., Nenes, A.,  
 941 Adams, P. J., Streets, D. G., Kumar, N., and Rind, D.: Climatic effects of 1950 - 2050  
 942 changes in US anthropogenic aerosols - Part 1: Aerosol trends and radiative forcing,  
 943 *Atmos. Chem. Phys.*, 12, 3333-3348, 10.5194/acp-12-3333-2012, 2012.  
 944 Lelieveld, J., Evans, J. S., Fnais, M., Giannadaki, D., and Pozzer, A.: The contribution of  
 945 outdoor air pollution sources to premature mortality on a global scale, *Nature*, 525, 367-  
 946 371, 10.1038/nature15371, 2015.  
 947 Li, Z., Niu, F., Fan, J., Liu, Y., Rosenfeld, D., and Ding, Y.: Long-term impacts of aerosols on  
 948 the vertical development of clouds and precipitation, *Nature Geosci.*, 4, 888-894, 2011.  
 949 Liu, S., Hua, S., Wang, K., Qiu, P., Liu, H., Wu, B., Shao, P., Liu, X., Wu, Y., Xue, Y., Hao,  
 950 Y., and Tian, H.: Spatial-temporal variation characteristics of air pollution in Henan of  
 951 China: Localized emission inventory, WRF/Chem simulations and potential source  
 952 contribution analysis, *Sci. Total Environ.*, 624, 396-406,  
 953 <https://doi.org/10.1016/j.scitotenv.2017.12.102>, 2018.  
 954 Lugauer, M., and Winkler, P.: Thermal circulation in South Bavaria – climatology and synoptic  
 955 aspects, *Meteor. Z.*, 14, 15-30, 2005.  
 956 Ma, N., Birmili, W., Müller, T., Tuch, T., Cheng, Y. F., Xu, W. Y., Zhao, C. S., and  
 957 Wiedensohler, A.: Tropospheric aerosol scattering and absorption over central Europe:  
 958 a closure study for the dry particle state, *Atmos. Chem. Phys.*, 14, 6241-6259,  
 959 10.5194/acp-14-6241-2014, 2014.  
 960 Marmer, E., and Langmann, B.: Aerosol modeling over Europe: 1. Interannual variability of  
 961 aerosol distribution, *J. Geophys. Res.*, 112, D23S15, doi:10.1029/2006JD008113, 2007.

Matthias, V., Arndt, J. A., Aulinger, A., Bieser, J., Denier van der Gon, H., Kranenburg, R.,  
 Kuenen, J., Neumann, D., Pouliot, G., and Quante, M.: Modeling emissions for three-  
 dimensional atmospheric chemistry transport models, *Journal of the Air & Waste*  
*Management Association*, 68, 763-800, 10.1080/10962247.2018.1424057, 2018.

Miller, M. S., Friedlander, S. K., and Hidy, G. M.: A chemical element balance for the Pasadena  
 aerosol, *J. Colloid Interface Sci.*, 39, 165-176, [https://doi.org/10.1016/0021-](https://doi.org/10.1016/0021-9797(72)90152-X)  
 9797(72)90152-X, 1972.

Minkos, A., Dauert, U., Feigenspan, S., and Kessinger, S.: . German Environment Agency, Jan  
 2019, D-06813 , 28 pp. , Accessed on September 6, 2019 [Online] Available:  
[https://www.umweltbundesamt.de/sites/default/files/medien/1410/publikationen/1903](https://www.umweltbundesamt.de/sites/default/files/medien/1410/publikationen/1903_29_uba_hg_luftqualitaet_engl_bf.pdf)  
 29\_uba\_hg\_luftqualitaet\_engl\_bf.pdf: Air Quality 2018 - Preliminary Evaluation,  
 German Environment Agency, Dessau-Rosslau, Germany, 28, 2019.

Monks, P. S., Archibald, A. T., Colette, A., Cooper, O., Coyle, M., Derwent, R., Fowler, D.,  
 Granier, C., Law, K. S., Mills, G. E., Stevenson, D. S., Tarasova, O., Thouret, V., von  
 Schneidemesser, E., Sommariva, R., Wild, O., and Williams, M. L.: Tropospheric ozone  
 and its precursors from the urban to the global scale from air quality to short-lived  
 climate forcer, *Atmos. Chem. Phys.*, 15, 8889-8973, 10.5194/acp-15-8889-2015, 2015.

Müller, T., Henzing, J. S., de Leeuw, G., Wiedensohler, A., Alastuey, A., Angelov, H., Bizjak,  
 M., Collaud Coen, M., Engström, J. E., Gruening, C., Hillamo, R., Hoffer, A., Imre, K.,  
 Ivanow, P., Jennings, G., Sun, J. Y., Kalivitis, N., Karlsson, H., Komppula, M., Laj, P.,  
 Li, S. M., Lunder, C., Marinoni, A., Martins dos Santos, S., Moerman, M., Nowak, A.,  
 Ogren, J. A., Petzold, A., Pichon, J. M., Rodriguez, S., Sharma, S., Sheridan, P. J.,  
 Teinilä, K., Tuch, T., Viana, M., Virkkula, A., Weingartner, E., Wilhelm, R., and Wang,  
 Y. Q.: Characterization and intercomparison of aerosol absorption photometers: result  
 of two intercomparison workshops, *Atmos. Meas. Tech.*, 4, 245-268, [10.5194/amt-4-](https://doi.org/10.5194/amt-4-245-2011)  
 245-2011, 2011.

988 Nordmann, S., Birmili, W., Weinhold, K., Müller, K., Spindler, G., and Wiedensohler, A.:  
 989 Measurements of the mass absorption cross section of atmospheric soot particles using  
 990 Raman spectroscopy, *J. Geophys. Res.*, 118, 12,075-012,085, 10.1002/2013JD020021,  
 991 2013.

992 Panagos, P., Borrelli, P., Poesen, J., Ballabio, C., Lugato, E., Meusburger, K., Montanarella,  
 993 L., and Alewell, C.: The new assessment of soil loss by water erosion in Europe,  
 994 *Environmental Science & Policy*, 54, 438-447, 10.1016/j.envsci.2015.08.012, 2015.

995 Patashnick, H., and Rupprecht, E. G.: Continuous PM-10 Measurements Using the Tapered  
 996 Element Oscillating Microbalance, *Journal of the Air & Waste Management*  
 997 *Association*, 41, 1079-1083, 10.1080/10473289.1991.10466903, 1991.

998 Penner, J. E., Dong, X., and Chen, Y.: Observational evidence of a change in radiative forcing  
 999 due to the indirect aerosol effect, *Nature*, 427, 231-234, 2004.

1000 Petzold, A., Ogren, J. A., Fiebig, M., Laj, P., Li, S. M., Baltensperger, U., Holzer-Popp, T.,  
 1001 Kinne, S., Pappalardo, G., Sugimoto, N., Wehrli, C., Wiedensohler, A., and Zhang, X.  
 1002 Y.: Recommendations for reporting "black carbon" measurements, *Atmos. Chem.*  
 1003 *Phys.*, 13, 8365-8379, 10.5194/acp-13-8365-2013, 2013.

1004 Pruppacher, H. R., and Klett, J. D.: *Microphysics of Clouds and Precipitation*, Reidel Publishing  
 1005 Co., Dordrecht, 714pp, 1978.

1006 Rehme, R.: Application of Gas Phase Titration in the Calibration of Nitric Oxide, Nitrogen  
 1007 Dioxide, and Ozone Analyzers, in: *Calibration in Air Monitoring*, edited by: Chapman,  
 1008 R., and Sheesley, D., ASTM International, West Conshohocken, PA, 198-209, 1976.

1009 Reitebuch, O., Dabas, A., Delville, P., Drobinsk, P., and Gantner, L.: Characterization of Alpine  
 1010 pumping by airborne Doppler lidar and numerical simulations., *Int. Conf. Alp. Meteor.*,  
 1011 *Brig 2003. – Publications of MeteoSwiss*, 66, 134-137, 2003.

1012 Riemer, N., Vogel, H., and Vogel, B.: Soot aging time scales in polluted regions during day  
 1013 and night, *Atmos. Chem. Phys.*, 4, 1885-1893, 2004.

1014 Rohde, R. A., and Muller, R. A.: Air Pollution in China: Mapping of Concentrations and  
1015 Sources, PLoS One, 10, e0135749-e0135749, 10.1371/journal.pone.0135749, 2015.

1016 Samset, B. H., Sand, M., Smith, C. J., Bauer, S. E., Forster, P. M., Fuglestad, J. S., Osprey,  
1017 S., and Schleussner, C. F.: Climate Impacts From a Removal of Anthropogenic Aerosol  
1018 Emissions, Geophysical Research Letters, 45, 1020-1029, 10.1002/2017gl076079,  
1019 2018.

1020 Schell, B., Ackermann, I., Hass, H., Binkowski, F., and Ebel, A.: Modeling the formation of  
1021 secondary organic aerosol within a comprehensive air quality model system, J.  
1022 Geophys. Res., 106, 28275–28293, 2001.

1023 Schwartz, S. E.: The whitehouse effect - shortwave radiative forcing of climate by  
1024 anthropogenic aerosols: an overview, J. Aerosol Sci., 27, 359-382, 1996.

1025 Sen, P. K.: Estimates of the Regression Coefficient Based on Kendall's Tau, J. Am. Stat.  
1026 Assoc., 63, 1379–1389, 1968.

1027 Spindler, G., Müller, K., and Herrmann, H.: Main particulate matter components in Saxony  
1028 (Germany) - trends and sampling aspects, Environ. Sci. Pollut. Res., 6, 89-94, 1999.

1029 Spindler, G., Grüner, A., Müller, K., Schlimper, S., and Herrmann, H.: Long-term size-  
1030 segregated particle (PM<sub>10</sub>, PM<sub>2.5</sub>, PM<sub>1</sub>) characterization study at Melpitz -- influence  
1031 of air mass inflow, weather conditions and season, J. Atmos. Chem., 70, 165-195,  
1032 10.1007/s10874-013-9263-8, 2013.

1033 Stein, A. F., Draxler, R. R., Rolph, G. D., Stunder, B. J. B., Cohen, M. D., and Ngan, F.:  
1034 NOAA's HYSPLIT Atmospheric Transport and Dispersion Modeling System, Bull.  
1035 Amer. Meteor. Soc., 96, 2059-2077, 10.1175/BAMS-D-14-00110.1, 2015.

1036 Stohl, A.: Trajectory statistics - a new method to establish source-receptor relationships of air  
1037 pollutants and its application to the transport of particulate sulfate in Europe, Atmos.  
1038 Environ., 30, 579-587, 1996.

- 1039 Stohl, A.: Computations, accuracy and applications of trajectories - A review and bibliography,  
1040 Atmos. Environ., 32, 947-966, 1998.
- 1041 Struzewska, J., and Jefimow, M.: A 15-year analysis of surface ozone pollution in the context  
1042 of hot spells episodes over Poland, Acta Geophysica, 64, 1875-1902, 10.1515/acgeo-  
1043 2016-0067, 2013.
- 1044 Sun, J., Birmili, W., Hermann, M., Tuch, T., Weinhold, K., Spindler, G., Schladitz, A., Bastian,  
1045 S., Löschau, G., Cyrys, J., Gu, J., Flentje, H., Briel, B., Asbach, C., Kaminski, H., Ries,  
1046 L., Sohmer, R., Gerwig, H., Wirtz, K., Meinhardt, F., Schwerin, A., Bath, O., Ma, N.,  
1047 and Wiedensohler, A.: Variability of Black Carbon Mass Concentrations, Sub-  
1048 micrometer Particle Number Concentrations and Size Distributions: Results of the  
1049 German Ultrafine Aerosol Network Ranging from City Street to High Alpine Locations,  
1050 Atmos. Environ., 202, 256-268, <https://doi.org/10.1016/j.atmosenv.2018.12.029>, 2019.
- 1051 Sun, J., Birmili, W., Hermann, M., Tuch, T., Weinhold, K., Merkel, M., Rasch, F., Müller, T.,  
1052 Schladitz, A., Bastian, S., Löschau, G., Cyrys, J., Gu, J., Flentje, H., Briel, B., Asbach,  
1053 C., Kaminski, H., Ries, L., Sohmer, R., Gerwig, H., Wirtz, K., Meinhardt, F., Schwerin,  
1054 A., Bath, O., Ma, N., and Wiedensohler, A.: Decreasing Trends of Particle Number and  
1055 Black Carbon Mass Concentrations at 16 Observational Sites in Germany from 2009 to  
1056 2018, Atmos. Chem. Phys., 2019, 1-19, 10.5194/acp-2019-754, 2020.
- 1057 Swietlicki, E., Svantesson, B., and Hansson, H.-C.: European source area apportionment, J.  
1058 Aerosol Sci., 19, 1175-1178, 1988.
- 1059 Theil, H.: A Rank-Invariant Method of Linear and Polynomial Regression Analysis, in: Henri  
1060 Theil's Contributions to Economics and Econometrics: Econometric Theory and  
1061 Methodology, edited by: Raj, B., and Koerts, J., Springer Netherlands, Dordrecht, 345-  
1062 381, 1992.
- 1063 Twomey, S.: Pollution and the planetary albedo, Atmos. Environ., 8, 1251-1256, 1974.

1064 van Pinxteren, D., Mothes, F., Spindler, G., Fomba, K. W., and Herrmann, H.: Trans-boundary  
 1065 PM10: Quantifying impact and sources during winter 2016/17 in eastern Germany,  
 1066 Atmos. Environ., 200, 119-130, <https://doi.org/10.1016/j.atmosenv.2018.11.061>, 2019.  
 1067 Wehner, B., Siebert, H., Stratmann, F., Tuch, T., Wiedensohler, A., Petäjä, T., Dal Maso, M.,  
 1068 and Kulmala, M.: Horizontal homogeneity and vertical extent of new particle formation  
 1069 events, Tellus, 59 B, 362-371, 2007.  
 1070 Wichmann, H. E., and Peters, A.: Epidemiological evidence of the effects of ultrafine particle  
 1071 exposure, Philosophical Transactions of the Royal Society of London, 358, 1751-2769,  
 1072 2000.  
 1073 Wiedensohler, A., Birmili, W., Nowak, A., Sonntag, A., Weinhold, K., Merkel, M., Wehner,  
 1074 B., Tuch, T., Pfeifer, S., Fiebig, M., Fjåraa, A. M., Asmi, E., Sellegri, K., Depuy, R.,  
 1075 Venzac, H., Villani, P., Laj, P., Aalto, P., Ogren, J. A., Swietlicki, E., Williams, P.,  
 1076 Roldin, P., Quincey, P., Hüglin, C., Fierz-Schmidhauser, R., Gysel, M., Weingartner,  
 1077 E., Riccobono, F., Santos, S., Gruning, C., Faloon, K., Beddows, D., Harrison, R.,  
 1078 Monahan, C., Jennings, S. G., O'Dowd, C. D., Marinoni, A., Horn, H. G., Keck, L.,  
 1079 Jiang, J., Scheckman, J., McMurry, P. H., Deng, Z., Zhao, C. S., Moerman, M., Henzing,  
 1080 B., de Leeuw, G., Löschau, G., and Bastian, S.: Mobility particle size spectrometers:  
 1081 harmonization of technical standards and data structure to facilitate high quality long-  
 1082 term observations of atmospheric particle number size distributions, Atmos. Meas.  
 1083 Tech., 5, 657-685, [10.5194/amt-5-657-2012](https://doi.org/10.5194/amt-5-657-2012), 2012.  
 1084 Wiedensohler, A., Wiesner, A., Weinhold, K., Birmili, W., Hermann, M., Merkel, M., Müller,  
 1085 T., Pfeifer, S., Schmidt, A., Tuch, T., Velarde, F., Quincey, P., Seeger, S., and Nowak,  
 1086 A.: Mobility particle size spectrometers: Calibration procedures and measurement  
 1087 uncertainties, Aerosol Sci. Technol., 52, 146-164, [10.1080/02786826.2017.1387229](https://doi.org/10.1080/02786826.2017.1387229),  
 1088 2018.  
 1089 Winkler, P., Lugauer, M., and Reitebuch, O.: Alpine Pumping, PROMET, 32, 34-42, 2006.

1090 Wolke, R., Hellmuth, O., Knoth, O., Schröder, W., Heinrich, B., and Renner, E.: The chemistry-  
 1091 transport modeling system LM-MUSCAT: Description and CityDelta applications, in:  
 1092 Air Pollution Modeling and its Application XVI, Kluwer Academic/Plenum, 427–439,  
 1093 2004.  
 1094 Zanatta, M., Gysel, M., Bukowiecki, N., Müller, T., Weingartner, E., Areskoug, H., Fiebig, M.,  
 1095 Yttri, K. E., Mihalopoulos, N., Kouvarakis, G., Beddows, D., Harrison, R. M., Cavalli,  
 1096 F., Putaud, J. P., Spindler, G., Wiedensohler, A., Alastuey, A., Pandolfi, M., Sellegri,  
 1097 K., Swietlicki, E., Jaffrezo, J. L., Baltensperger, U., and Laj, P.: A European aerosol  
 1098 phenomenology-5: Climatology of black carbon optical properties at 9 regional  
 1099 background sites across Europe, Atmos. Environ., 145, 346-364,  
 1100 10.1016/j.atmosenv.2016.09.035, 2016.  
 1101 Zhu, K., Zhang, J., and Lioy, P. J.: Evaluation and Comparison of Continuous Fine Particulate  
 1102 Matter Monitors for Measurement of Ambient Aerosols, Journal of the Air & Waste  
 1103 Management Association, 57, 1499-1506, 10.3155/1047-3289.57.12.1499, 2007.

1104

Formatiert: Einzug: Links: 0 cm, Hängend: 1.25 cm



Table 1: Characteristics of the four stations of the present study, see text for instrumental details. The number of validated data hours is given for each component

Station	Acronym	Latitude	Longitude	MPSS <sup>1</sup>	eBC <sup>2</sup>	PM10 <sup>3</sup>	PM10 <sup>4</sup>	NO <sub>x</sub> <sup>6</sup>	SO <sub>2</sub> <sup>7</sup>	O <sub>3</sub> <sup>8</sup>
						continuous <sup>3,4</sup>	discontinuous <sup>5</sup>			
Collmberg	CO	51.3	13			85054		88838		88792
Melpitz	ME	51.5	12.9	81561	88196		88822	86260	85541	84421
Neuglobsow	NG	53.1	13	57962	77540	71202		83718	87778	87943
Waldhof	WA	52.8	10.8	84276	80725	88321		85503	82386	87373

<sup>1</sup>MPSS - scanning mobility particle size spectrometer TROPOS (10 – 800 nm); <sup>2</sup>MAAP - Multi-angle absorption photometer 5012 Thermo Fischer Scientific; <sup>3</sup>TEOM-FDM - Tapered element oscillating microbalance fitted with a filter dynamics measuring system 1405 Thermo Fischer Scientific; <sup>4</sup>SCHARP - Synchronized Hybrid Ambient Real-time Particulate Monitor 5030 Thermo Fischer Scientific; <sup>5</sup>HVS – High Volume Sampler DIGITEL DH-80; <sup>6</sup>TLA-NO<sub>x</sub> –Trace Level NO<sub>x</sub> Analyzer 42i-TL Thermo Fischer Scientific; <sup>7</sup>TLA-SO<sub>2</sub> - Trace Level SO<sub>2</sub> Analyzer 43i-TLE Thermo Fischer Scientific; <sup>8</sup>

Table 2 Median concentrations of eBC concentrations ( $\mu\text{g m}^{-3}$ ) and temporal trends (2009-2018) of eBC in terms of Sen-Theil slope (% per year) as determined for air masses passing over Regions A and B as analyzed at the stations Melpitz (ME), Neuglobsow (NG), and Waldhof (WA). For comparison the national annual decreases in BC emissions 2009-2017 in % according to the European Environmental Agency are added.

	<u>DELTA</u>			Median eBC in							Decrease in national BC emissions			
	<u>T*</u> in h	No. of back trajectories			$\mu\text{m/m}^3$			Sen-Theil slope in % per year				in % per year		
		<u>ME</u>	<u>NG</u>	<u>WA</u>	<u>ME</u>	<u>NG</u>	<u>WA</u>	<u>ME</u>	<u>NG</u>	<u>WA</u>	<u>3 Stations**</u>	<u>Belgium</u>	<u>Netherlands</u>	<u>Germany</u>
	1	21941	17514	27218	0.38	0.40	0.41	6.40	6.80	4.80	-5.85	-6.1%	-6.1%	-4.9%
Region A	3	18605	14268	22132	0.38	0.40	0.41	6.40	6.90	4.80	-5.89			
B-NL-NRW	6	14802	10086	15936	0.39	0.40	0.42	6.40	7.60	5.10	-6.19			
	12	6817	3746	6131	0.40	0.50	0.50	7.10	7.90	5.30	-6.62			
												<u>Czech Rep.</u>	<u>Poland</u>	<u>Slovakia</u>
	1	11096	5264	4191	1.10	1.19	1.13	3.60	3.40	1.70	-3.16	-2.8%	0.5%	-2.3%
Region B	3	9601	4339	3541	1.08	1.18	1.12	3.40	3.40	2.10	-3.14			
CZ-PL-SK	6	7000	3062	2570	1.05	1.09	1.11	4.00	2.90	2.70	-3.47			
	12	3628	1410	1277	1.00	1.00	1.00	3.70	3.00	2.70	-3.34			
ALL		85846	75190	78356	0.45	0.36	0.36	5.90	5.60	4.00	-5.18			
Sun (2020)								4.40	7.80	3.20				

\* Minimum time spent over the specified source region, \*\*Weighted mean, according to the available number of back trajectories

Formatiert: Schriftart: (Standard) Times New Roman

Formatiert: Schriftart: (Standard) Times New Roman

Formatiert: Schriftart: (Standard) Times New Roman

Formatiert: Schriftart: (Standard) Times New Roman

Formatiert: Schriftart: (Standard) Times New Roman

Formatiert: Schriftart: (Standard) Times New Roman

Formatiert: Schriftart: (Standard) Times New Roman

Formatiert: Schriftart: (Standard) Times New Roman

Formatiert: Schriftart: (Standard) Times New Roman

Formatiert: Schriftart: (Standard) Times New Roman

Formatiert: Schriftart: (Standard) Times New Roman

Formatiert: Schriftart: (Standard) Times New Roman

Formatiert: Schriftart: (Standard) Times New Roman

Formatiert: Schriftart: (Standard) Times New Roman

Formatiert: Schriftart: (Standard) Calibri, 11 Pt.,  
Schriftfarbe: Schwarz

Formatiert: Einzug: Links: 0 cm, Erste Zeile: 0 cm,  
Zeilenabstand: einfach

Table 3 Percental decreases in the anthropogenic emissions of PM<sub>10</sub>, BC, SO<sub>2</sub>, and NO<sub>x</sub> relative to 2009 as reported by the European Environment Agency (EEA, <https://www.eea.europa.eu/data-and-maps/dashboards/air-pollutant-emissions-data-viewer-2>), the German Environment Agency (GEA), and calculated in the present study. The EEA and GEA only report data until 2017, (\*=BC until 2016).

Component	EEA	GEA	<del>GUAN</del> <del>emissions</del> <del>2009-</del> 2017	<del>GUAN</del> <del>emissions</del> <del>2009-</del> <del>2018</del>
	2009- 2017	2009- 2017		
PM <sub>10</sub>	12%	4.2%	16%	6%
BC*	29%	35%*	63%	44%
SO <sub>2</sub>	33%	20%	68%	59%
NO <sub>x</sub>	20%	11%	43%	30%

Gelöscht: .....Seitenumbruch.....

Gelöscht: 2

Gelöscht: Present study

Gelöscht: until

Gelöscht: Present study until 2018

Formatierte Tabelle

Gelöscht: ¶

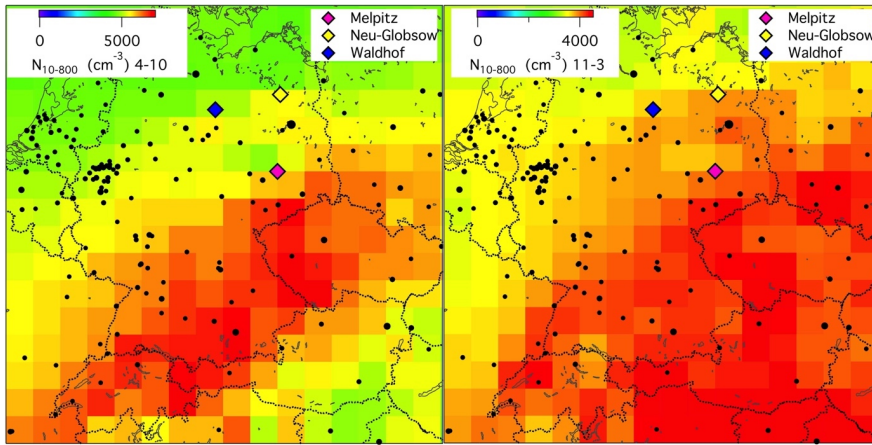
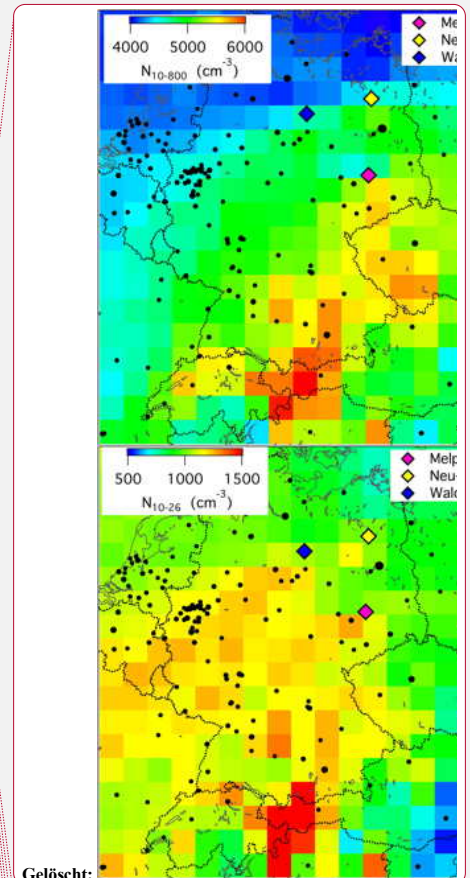


Fig. 1 Maps of particle number concentration  $N_{10-800}(\text{cm}^{-3})$  extrapolated under 1000 m height along five day back trajectories from hourly data at the four stations from 2009 to 2018; left: months April through October; right: months November through March. The GUAN-stations are marked with colored diamonds. The Collmberg station lies 30 km Southeast of station Melpitz. Here and in the following maps the black dots represent cities larger than 100000 inhabitants with the size of the dots being proportional to the number of inhabitants.



Gelöscht:

Gelöscht: (top left,  $N_{10-800}$ ,

Formatiert: Tiefgestellt

Gelöscht: s

Gelöscht: , and below 26 nm diameter (bottom left,  $N_{10-26}$ ,  $\text{cm}^{-3}$ )

Gelöscht: ,

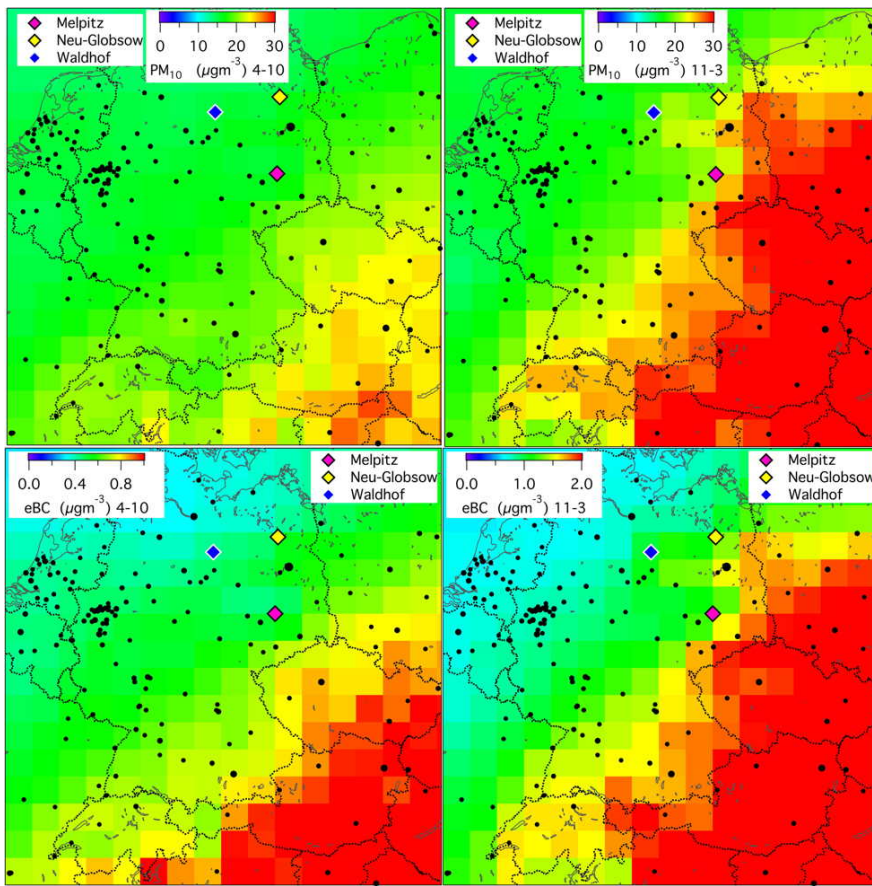


Fig. 2 As Fig. 1 but for particle mass concentrations (top,  $\text{PM}_{10}$ ,  $\mu\text{gcm}^{-3}$ ), and black carbon concentrations (bottom,  $\text{eBC}$ ,  $\mu\text{gcm}^{-3}$ ).

Formatiert: Zentriert

Gelöscht: volume

Gelöscht: right

Gelöscht: right

**Gelöscht:** ), extrapolated along back trajectories from hourly data at the four stations from 2009 to 2018. The GUAN-stations are marked with colored diamonds. The Collnberg station lies 30 km Southeast of station Melpitz. Here and in the following maps the black dots represent cities larger than 100000 inhabitants with the size of the dots being proportional to the number of inhabitants.



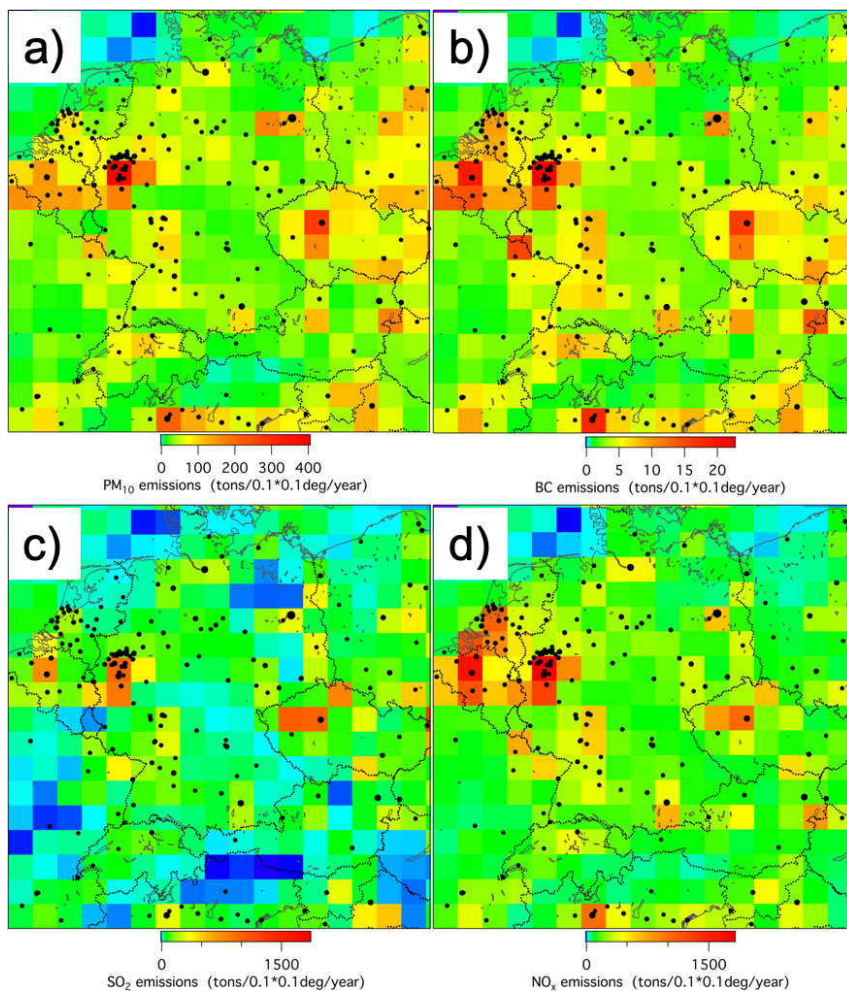
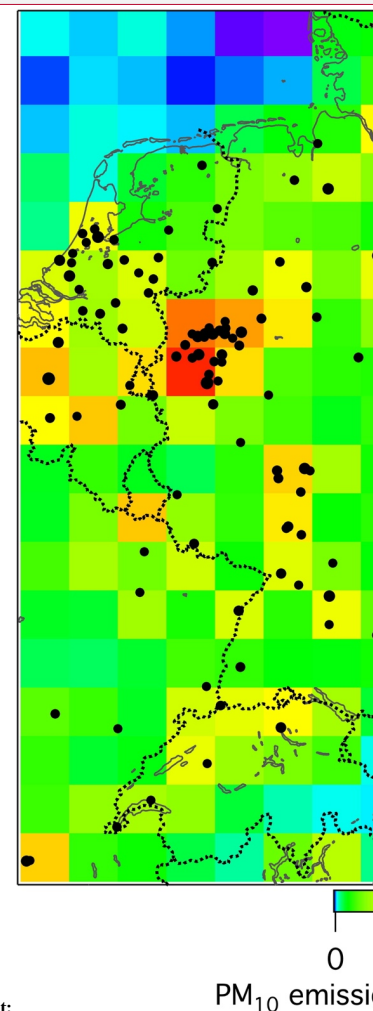


Fig. 3 As Fig. 1 but a) for PM<sub>10</sub> emissions (tons/0.1\*0.1deg./year), b) for BC emissions, c) for SO<sub>2</sub> emissions, and d) for NO<sub>x</sub> emissions (tons/0.1\*0.1deg./year) according to the EDGAR emission database ([https://data.europa.eu/doi/10.2904/JRC\\_DATASET\\_EDGAR](https://data.europa.eu/doi/10.2904/JRC_DATASET_EDGAR)) for 2009 averaged over the geogrid of the present study.



Gelöscht:  
Gelöscht: 2  
Formatiert: Tiefgestellt  
Gelöscht:  
Formatiert: Tiefgestellt

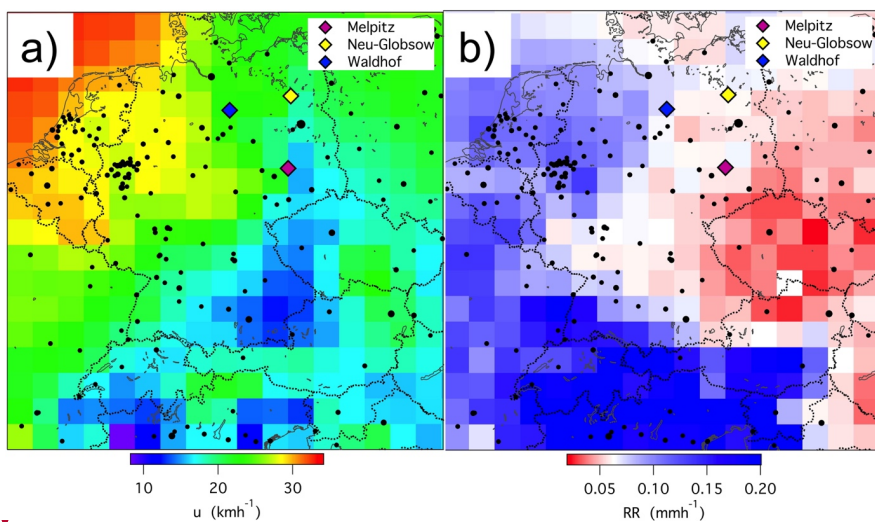
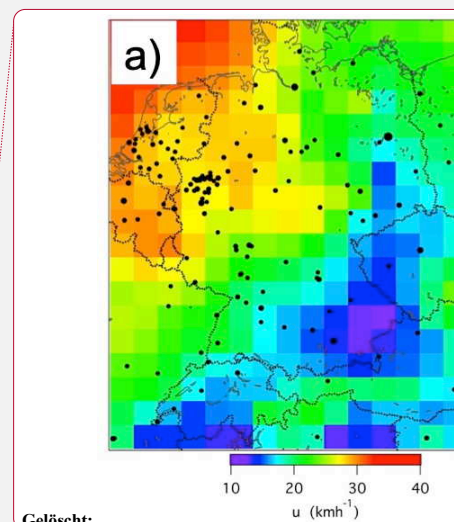


Fig. 4 a) Map of horizontal wind speed ( $u$ ,  $\text{kmh}^{-1}$ ) as reported by HYSPLIT along hourly five-day back trajectories to the four stations marked in the graph averaged over the time period 2009 to 2018; b) as a) but for precipitation ( $RR$ ,  $\text{mmh}^{-1}$ ).



Gelöscht:

Gelöscht: 3

Gelöscht: Map

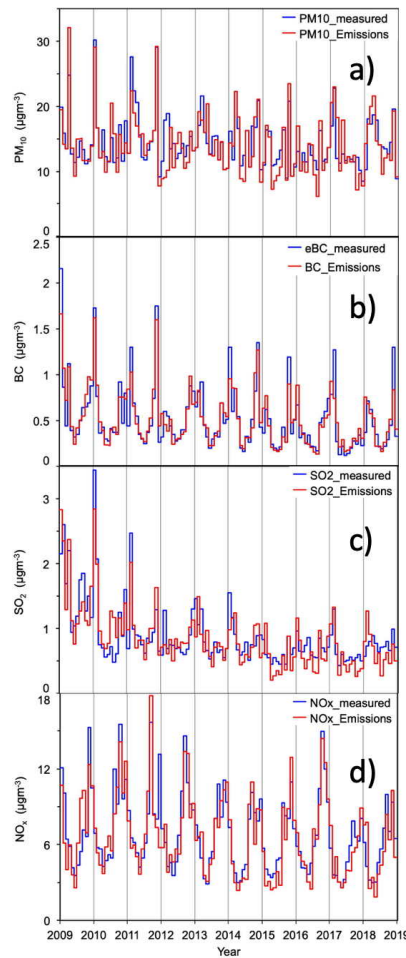


Fig. 5 a) Monthly medians of PM<sub>10</sub>-concentrations at the four stations of the present study (blue), and monthly medians of optimized sums of PM<sub>10</sub>-emissions along back trajectories leading to the stations (red). b) as a) but for measured eBC-concentrations and BC-emissions along back trajectories. c) as a) but for measured SO<sub>2</sub>-concentrations and SO<sub>2</sub>-emissions along back trajectories. d) as a) but for measured NO<sub>x</sub>-concentrations and NO<sub>x</sub> -emissions along back trajectories.

Gelöscht: 4



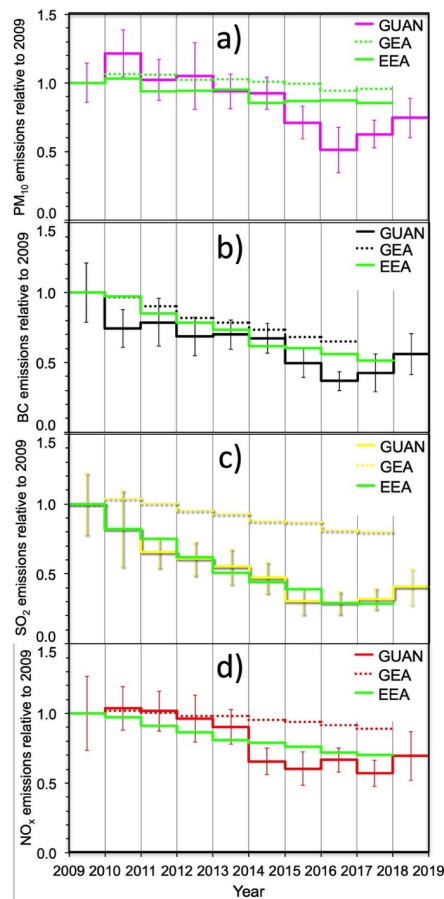
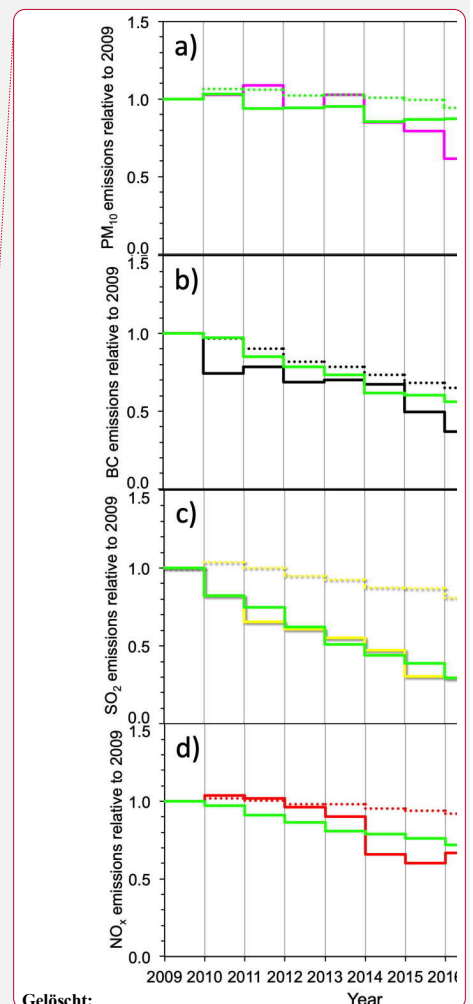


Fig. 6 GUAN: Trends in the emissions of a) PM<sub>10</sub>, b) BC, c) SO<sub>2</sub>, and d) NO<sub>x</sub>, relative to 2009

as calculated by optimizing the agreement between 2009-EDGAR-emissions and concentrations measured at the four stations of the present study. The error bars represent annual average relative deviations between measured and simulated data.

GEA: Trends as reported for Germany by the German Environment Agency. EEA: Trends as optimized from combinations of trends over Germany and neighboring countries, (see text for details).

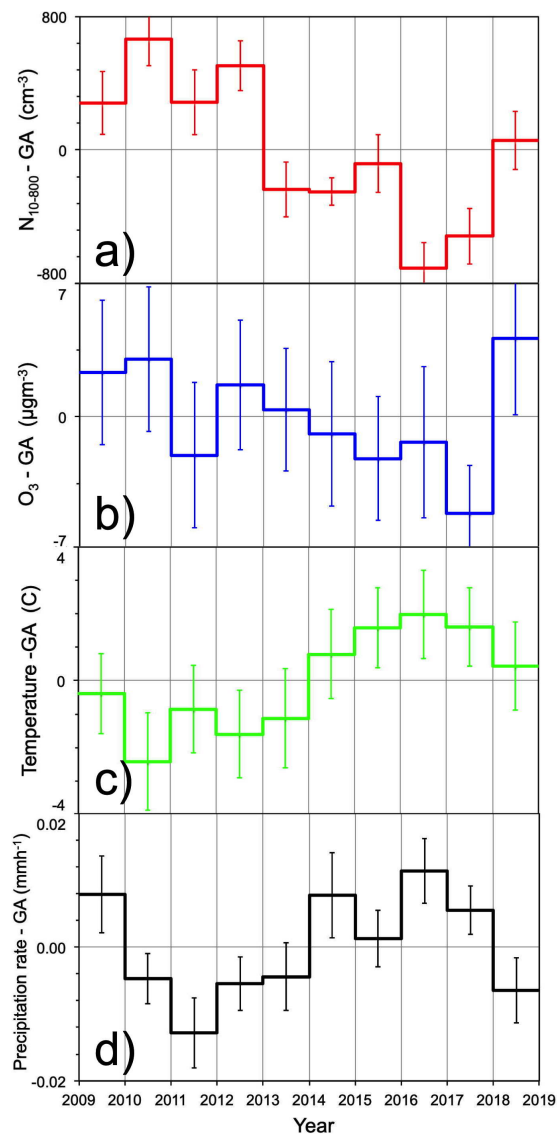


Gelöscht:

Gelöscht: 5

[2] nach unten verschoben: The error bars represent annual average relative deviations between measured and simulated data.

[2] verschoben (Einfügung)



Formatiert: Zentriert

Fig. 7 Trends in annual average deviations a)  $\Delta N_{10-800}$ , b)  $\Delta O_3$ , c) temperature  $\Delta T$  along the trajectories five days back in time, and d) precipitation rate  $\Delta RR$  along the trajectories three days back in time. The deviations are taken relative to the respective 10-year

Formatiert: Schriftart: Symbol

1252  
1253  
1254

Grand Average (GA). The error bars represent the standard deviations of the annual averages.

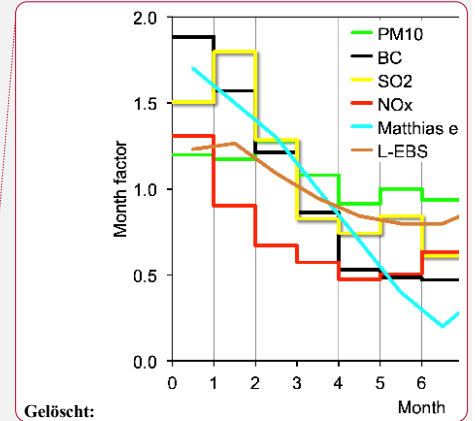
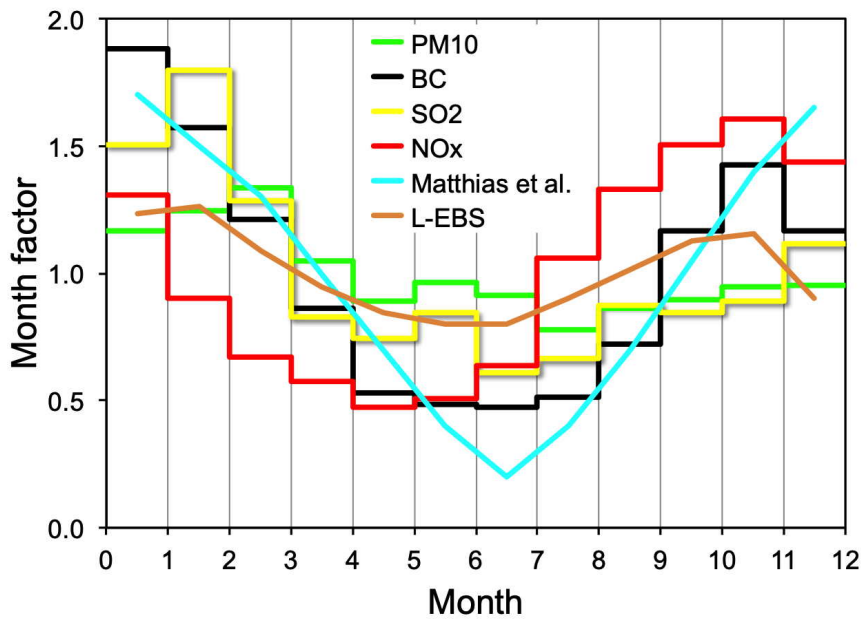


Fig. 8 Month factors for the emissions of PM<sub>10</sub>, BC, SO<sub>2</sub>, and NO<sub>x</sub> as determined by optimizing the agreement between EDGAR-emissions and concentrations measured at the four stations of the present study. For comparison the month factors of Matthias et al., (2018) for combustion emissions are plotted and the relative annual variation of eBC concentrations measured at the station Leipzig-Eisenbahnstraße (L-EBS) averaged over the time period of the present study.

Gelöscht: 6

Seite 40: [1] Gelöscht	Nemo	01.04.20 11:58:00
------------------------	------	-------------------

Seite 40: [2] Formatiert	Nemo	01.04.20 11:58:00
--------------------------	------	-------------------

Rechts: 2 cm, Unten: 2.5 cm, Breite: 29.66 cm, Höhe: 20.99 cm

Seite 40: [3] Formatierte Tabelle	Nemo	30.04.20 11:06:00
-----------------------------------	------	-------------------

Formatierte Tabelle

Seite 40: [4] Gelöscht	Nemo	01.04.20 11:49:00
------------------------	------	-------------------



Seite 40: [4] Gelöscht	Nemo	01.04.20 11:49:00
------------------------	------	-------------------



Seite 40: [5] Formatiert	Nemo	02.04.20 15:32:00
--------------------------	------	-------------------

Schriftart: 12 Pt.

Seite 40: [6] Formatiert	Nemo	02.04.20 15:32:00
--------------------------	------	-------------------

Schriftart: 12 Pt.

Seite 40: [7] Formatiert	Nemo	30.04.20 11:06:00
--------------------------	------	-------------------

Tiefgestellt

Seite 40: [7] Formatiert	Nemo	30.04.20 11:06:00
--------------------------	------	-------------------

Tiefgestellt

Seite 40: [8] Formatiert	Nemo	02.04.20 15:32:00
--------------------------	------	-------------------

Schriftart: 12 Pt.

Seite 40: [8] Formatiert	Nemo	02.04.20 15:32:00
--------------------------	------	-------------------

Schriftart: 12 Pt.

Seite 40: [9] Formatiert	Nemo	02.04.20 15:32:00
--------------------------	------	-------------------

Schriftart: 10 Pt.

Seite 40: [10] Formatiert	Nemo	02.04.20 15:32:00
---------------------------	------	-------------------

Schriftart: 10 Pt.

Seite 40: [11] Formatiert	Nemo	30.04.20 11:07:00
---------------------------	------	-------------------

Hochgestellt

Seite 40: [11] Formatiert	Nemo	30.04.20 11:07:00
---------------------------	------	-------------------

Hochgestellt